J. Membrane Biol. 125, 63–79 (1992)

The Journal of
Membrane Biology
© Springer-Verlag New York Inc. 1992

Electrogenic Properties of the Cloned Na^+/Glucose Cotransporter: II. A Transport Model under Nonrapid Equilibrium Conditions

Lucie Parent, Stéphane Supplisson, Donald D.F. Loo, and Ernest M. Wright
Department of Physiology, University of California at Los Angeles School of Medicine, Center for the Health Sciences, Los Angeles, California 90024-1751

Summary. The results of the accompanying electrophysiological study of the cloned Na^+/glucose cotransporter from small intestine (Parent, L., Supplisson, S., Loo, D.D.F., Wright, E.M. (1992) *J. Membrane Biol.* **125**:49–62) were evaluated in terms of a kinetic model. The steady-state and presteady-state cotransporter properties are described by a 6-state ordered kinetic model ("mirror" symmetry) with a Na^+:αMDG stoichiometry of 2. Carrier translocation in the membrane as well as Na^+ and sugar binding and dissociation are treated as a function of their individual rate constants. Empty carrier translocation and Na^+ binding/dissociation are the only steps considered to be voltage dependent. Currents were associated with the translocation of the negatively charged carrier in the membrane. Negative membrane potential facilitates sugar transport. One numerical solution was found for the 14 rate constants that account quantitatively for our experiment observations: i.e., (i) sigmoidal shape of the sugar-specific current-voltage curves (absence of outward currents and inward current saturation at high negative potentials), (ii) Na^+ and voltage dependence of $K_{0.5}^{sugar}$ and i_{max}^{sugar}, (iii) sugar and voltage dependence of $K_{0.5}^{Na}$ and i_{max}^{Na}, (iv) presteady-state currents and their dependence on external Na^+, αMDG and membrane potential, and (v) and carrier Na^+ leak current. We conclude that the main voltage effect is on carrier translocation. Na^+ ions that migrate from the extracellular medium to their binding sites sense 25 to 35% of the transmembrane voltage, whereas charges associated with the carrier translocation experiences 60 to 75% of the membrane electrical field. Internal Na^+ ion binding is not voltage dependent. In our nonrapid equilibrium model, the rate-limiting step for sugar transport is a function of the membrane potential, $[Na]_o$ and $[\alpha MDG]_o$. At 0 mV and at saturating $[Na]_o$ and $[\alpha MDG]_o$, the rate-limiting step for sugar transport is the empty carrier translocation (5 sec^{-1}). As the membrane potential is made more negative, the empty carrier translocation gets faster and the internal Na^+ dissociation becomes increasingly rate limiting. However, as $[Na]_o$ is decreased to less than 10 mM, the rate-limiting step is the external Na^+ ions binding in the 0 to −150 mV potential range. At 0 mV, the external Na^+ dissociation constant KNa' is 80 mM and decreases to 24 mM at −150 mV. The external sugar dissociation constant $KNaS'$ is estimated to be 200 μM and voltage independent. Finally, the internal leak pathway (CNa_2 translocation) is insignificant. While we cannot rule out a more complex kinetic model, the electrical properties of the cloned Na^+/glucose cotransporter are found to be adequately described by this 6-state kinetic model.

Key Words Na^+/glucose cotransport · electrogenic transporters · kinetic model · nonrapid equilibrium · presteady-state kinetics

Introduction

Transport studies of cotransport mechanisms have so far been limited to steady-state analysis. The identification of the rate-limiting steps and of the voltage dependence (translocation and/or Na^+ binding), and the values of the rate constants of the elementary reactions have yet to be resolved. The cloning and expression of membrane transport proteins has revitalized interest in transport kinetics. In the case of the intestinal brush-border Na^+/glucose cotransporter, the expression of the clone in *Xenopus laevis* oocytes has provided unique information regarding the voltage dependence of steady-state kinetics and presteady-state currents (Umbach, Coady & Wright, 1990; Parent et al., 1991*a*). In addition, the Na^+/glucose cotransporter expressed in oocytes exhibits internal Na^+ leak currents (Umbach et al., 1990; Parent et al., 1991*a*). In the companion paper, we described the kinetics of the cotransporter currents as a function of extracellular Na^+ and sugar concentrations over a large range of membrane potential. The results were presented in terms of presteady-state currents and steady-state kinetics. In this paper, we propose a simple kinetic model that accounts for the global electrical properties of the cloned Na^+/glucose cotransporter. A single set of numerical rate constants was found to describe adequately the sigmoidal shape of the current-voltage (*I-V*) relationships, the Na^+, sugar and voltage dependence of the steady-state kinetics parameters $K_{0.5}$ and i_{max}, the time course of the presteady-state currents and the Na^+ carrier leak currents. While the goodness of the fit does not eliminate more complex

kinetic models, the present analysis provides insights in the mechanism of Na^+/sugar transport which in turn casts a framework for the design of future experiments. Parts of this work have been presented earlier (Parent et al., 1991*b*).

Transport Model

Figure 1 shows our minimal model for the Na^+/glucose cotransporter, i.e., with the least free parameters required to account for the cotransporter steady-state and presteady-state electrical properties. This model is described as a 6-state[1] ordered model with "mirror" symmetry with external Na^+ ions binding first to the carrier ("last on-first off") (Segel, 1975). It consists of two transport loops linking six discrete states of the carrier. The carrier C possesses two binding sites for the driving ion Na^+ and one binding site for the sugar S (S = αMDG). Phlorizin binds to the CNa_2 carrier state to form an inactive complex CNa_2Pz'. The carrier is assumed to bear a charge $z = -2$ with the result that the Na^+-loaded carrier is electroneutral. The state transitions include three transmembrane steps: one charge-transport step $C' \rightleftharpoons C''$, one ternary complex translocation $CNa_2' \rightleftharpoons CNa_2''$ in the absence of sugar (carrier Na^+ leak), and one fully loaded carrier translocation $CNa_2S' \rightleftharpoons CNa_2S''$. In addition, there are individual steps for binding of Na^+ and sugar at each side of the membrane. The transport model is ordered in that two Na^+ ions bind to the carrier before sugar can bind.[2] The current is carried by the empty form of the carrier ($C'' \rightleftharpoons C'$) while translocation $CNa_2' \rightleftharpoons CNa_2''$ and $CNa_2S' \rightleftharpoons CNa_2S''$ are electrically silent. Membrane surface charges and unstirred layer effects at the membrane boundaries (Roomans & Borst-Pauwels, 1978) were assumed to be negligible, i.e., the substrate and cosubtrate concentrations were considered uniformly distributed between the membrane surface and the bulk aqueous phase. Each reaction step is a first or pseudo first-order process. Both Na^+ binding and carrier translocation may be voltage dependent. Rapid equilibrium was not assumed, and so each of the seven reaction steps is treated as a function of its individual rate constants.

Rationale

The minimal model that can be proposed to describe the properties of the Na^+/glucose cotransporter is a 4-state model with only two translocation steps: $C' \rightleftharpoons C''$ and $CNa_2S' \rightleftharpoons CNa_2S''$ and equilibrium binding of Na^+ and sugar. Two Na^+ ion binding sites were inferred from the coupling coefficient n of 2 Na^+ : 1 αMDG obtained from the relationship between carrier currents and $[Na]_o$ (*see* Hill plot Fig. 5, Parent et al., 1991*a*).

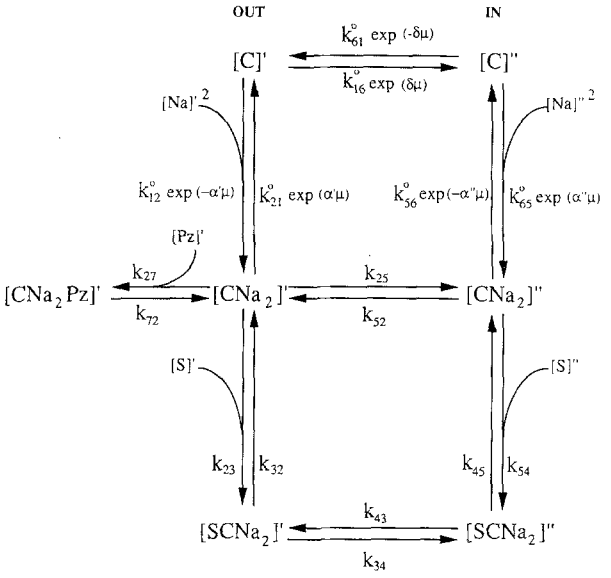

Fig. 1. Transport model for the Na^+/glucose cotransporter. Electrical properties of the cotransporter are described by a 6-state transport model with the empty carrier bearing two negative charges. Each carrier state was identified by a number from 1 to 6, and external and internal faces of the membrane were represented by $C_1 = C'$, $C_2 = CNa_2'$, $C_3 = CNa_2S'$, $C_4 = CNa_2S''$, $C_5 = CNa_2''$, $C_6 = C''$. Rate constants k_{12}, k_{21}, k_{16}, k_{61}, k_{56}, and k_{65} are described by voltage-independent values (k^0_{ij}) modulated by potential and/or ligand concentration (*see* Eqs. (12) to (25) and the Appendix). Phlorizin binds to the Na^+-loaded carrier CNa_2' to form the inactive CNa_2Pz' complex. Phlorizin inhibits sugar transport in the presence of external Na^+ with a K_i of 10 μM reflected by the rate constants k_{27} and k_{72}. It is not yet known if phlorizin can bind to the Na^+-loaded form CNa_2'' of the carrier. The loaded carrier is neutral and therefore not influenced by the membrane potential. α' and α'' are phenomenological constants that describe the fraction of the electrical field sensed by the Na^+ binding to its external and internal sites, respectively. δ is the fraction of the electrical field sensed by the empty ion binding site on the carrier during membrane translocation with $\alpha' + \alpha'' + \delta = 1$. μ is the electrochemical potential FV/RT. The sugar transport occurs only in presence of two Na^+ ions that bind first to the empty carrier.

The observation of phlorizin-sensitive Na^+-dependent currents in the absence of sugar (Umbach et al., 1990; Parent et al., 1991*a*) suggests that translocation of CNa_2 complexes requires a third membrane translocation step. On the contrary, sugar-dependent steady-state currents were not observed in the absence of external Na^+ (choline replacement) which indicates that formation and translocation of the CS complex is negligible in the absence of $[Na]_o$. The absence of sugar-dependent current in the absence of $[Na]_o$ is also supported by irradiation-inactivation studies performed on brush-border membrane vesicles (BBMV) which have shown that Na^+-independent sugar transport is insensitive to radiation. This suggests that Na^+-independent sugar transport measured in BBM is unlikely to be mediated by the cotransporter (Stevens et al., 1990).

[1] The number of 6 states refer to the number of states that actually contribute (directly) to sugar transport. The 7th state is the phlorizin-bound CNa_2Pz' complex which is not translocated (inert state) and was not included in our simulations.

[2] In our model, the binding of two Na^+ ions to the carrier is described as a single reaction step. This may imply that binding of the first Na^+ ion to the carrier is in rapid equilibrium (faster than any other rate) and that binding of the second Na^+ ion to the carrier is rate limiting. An alternative explanation is that there are two identical binding sites for Na^+ ions with similar rate constants.

Both Na^+ binding and carrier translocation may be voltage dependent which is implied by the voltage dependence of both $K_{0.5}^{Na}$ and i_{max}^{Na} (Fig. 6, Parent et al., 1991*a*). The absence of voltage dependence of $K_{0.5}^{\alpha MDG}$ observed at saturating $[Na]_o$ (Fig. 4, Parent et al., 1991*a*) indicates that sugar binding under these conditions is not voltage dependent.

The empty Na^+/glucose cotransporter bears two negative charges. It has already been postulated that the Na^+/glucose cotransporter is negatively charged in the absence of Na^+ ions (Aronson, 1978; Kessler & Semenza, 1983; Restrepo & Kimmich, 1985*b*; Lapointe, Hudson & Schultz, 1986; Schultz, 1986). The first evidence was obtained by Aronson (1978) who reported that phlorizin binding to renal BBMVs was voltage dependent.[3] These results were also confirmed by Turner and Silverman (1981).

We chose an ordered binding model in which two Na^+ ions bind to the cotransporter prior to sugar association. This means that sugar binding is only possible in the presence of CNa_2. The choice of an ordered binding model over a random binding model was made to keep the model as simple as possible.[4] However, an ordered binding mechanism is compatible with the large allosteric effect of $[Na]_o$ observed experimentally for $K_{0.5}^{\alpha MDG}$ (Fig. 4, Parent et al., 1991*a*) and would explain the voltage dependence of $K_{0.5}^{\alpha MDG}$ at low $[Na]_o$ as a consequence of the voltage dependence of Na^+ binding to the carrier.

There were previous reports of ordered binding mechanism describing the kinetic properties of the Na^+/glucose cotransporter in rabbit intestinal BBMV (Hopfer & Groseclose, 1980; Kessler & Semenza, 1983; Kaunitz & Wright, 1984) and in chicken intestinal cells (Restrepo & Kimmich, 1985*a*). An ordered binding mechanism was also suggested by reports from Peerce and Wright (1984, 1987) of a Na^+-induced conformational change preceding sugar binding to the Na^+/glucose cotransporter.

Na^+ and sugar rapid equilibrium binding is not assumed. Individual rate constants were used to describe each and every reaction step including sugar and Na^+ ions binding (Fig. 1). Because it reduces the complexity of the algebra required to model cotransport activity, the rapid equilibrium assumption has been the most enduring working hypothesis in cotransporter kinetic analysis (*see* for instance, Goldner, Schultz & Curran, 1969; Jauch & Läuger, 1986). Although it appears to be almost a universal assumption, exceptions can be found. For instance, Hopfer and Groseclose (1980) have proposed a kinetic model for the Na^+/glucose cotransporter in small intestine where the rate constant for translocation is at least six times slower than the dissociation of Na^+ ions at the extracellular interface. In addition, the rapid equilibrium assumption has been periodically questioned (e.g., Sanders et al., 1984; Sanders 1986; Schultz, 1986; Wierzbicki, Berteloot & Roy, 1990).

The density of cotransporters (C_T) was estimated to be around 50,000 carriers μm^{-2} (5×10^{10} carriers oocyte^{-1}). In a previous study, the Na^+/glucose cotransporter density in *Xenopus* oocytes was estimated to be between 50,000 and 200,000 carriers μm^{-2} (Umbach et al., 1990). This carrier density is similar to the estimated cotransporter density in intestinal brush-border membranes (Peerce & Wright, 1984) and similar to the reported surface density of other membrane proteins such as 10,000 μm^{-2} for ACh nicotinic receptors and 50,900 μm^{-2} for the *Halobacterium* rhodopsin (Hille, 1984).

[3] This explanation is valid only if one assumes the phlorizin-bound complex is not translocated.

[4] With a 8-state random binding model, the number of King Altman patterns increases from 15 to 50 with a total of 300 terms.

Formal Description

The variation of each carrier state as a function of time is described by the difference of the forward and backward reactions. To simplify the writing, $C_1 = C'$, $C_2 = CNa_2'$, $C_3 = CNa_2S'$, $C_4 = CNa_2S''$, $C_5 = CNa_2''$ and $C_6 = C''$. The set of differential equations with $n = 2$, is the following:

$$dC_1/dt = (k_{21}C_2 + k_{61}C_6) - (k_{12} + k_{16})C_1 \quad (1)$$

$$dC_2/dt = (k_{12}C_1 + k_{32}C_3 + k_{52}C_5) - (k_{21} + k_{23} + k_{25})C_2 \quad (2)$$

$$dC_3/dt = (k_{23}C_2 + k_{43}C_4) - (k_{32} + k_{34})C_3 \quad (3)$$

$$dC_4/dt = (k_{34}C_3 + k_{54}C_5) - (k_{45} + k_{43})C_4 \quad (4)$$

$$dC_5/dt = (k_{45}C_4 + k_{65}C_6 + k_{25}C_2) - (k_{54} + k_{52} + k_{56})C_5 \quad (5)$$

$$dC_6/dt = (k_{16}C_1 + k_{56}C_5) - (k_{61} + k_{65})C_6. \quad (6)$$

The total concentration of carrier in the membrane is constant:

$$C_T = C_1 + C_2 + C_3 + C_4 + C_5 + C_6 \quad (7)$$

therefore

$$dC_1/dt + dC_2/dt + dC_3/dt + dC_4/dt + dC_5/dt + dC_6/dt = 0. \quad (8)$$

The steady-state concentrations of individual carrier states (C_1, C_2, ...) were solved using the King and Altman (1956) diagrammatic method (*see* Appendix). The King-Altman method allows the concentration of any given carrier state C_x ($x = 1, 2, \ldots 6$) to be written solely in terms of rate constants and C_T. The concentration of C_x is given by the sum of 15 King-Altman (KA) patterns, each one being the product of five different rate constants. When C_x is expressed as a King-Altman term (KAT), it is denoted as KAT_i^j. The steady-state fraction of a given carrier state C_x is given by:

$$\frac{C_x}{C_T} = \frac{\sum_{j=1}^{15} KAT_x^j}{\sum_{i=1}^{6}\sum_{j=1}^{15} KAT_i^j} \quad (9)$$

where x is a given carrier state, i is a carrier state (1 to 6) and j is a King Altman pattern (1 to 15). The rate equations for each carrier state are given in details in Appendix.

In a 6-state model with three membrane translocation steps, the general equation for the steady-state sugar-dependent carrier current is given by the sum of all possible membrane translocation steps:

$$i = -F[z(k_{16}C_1 - k_{61}C_6) + (z + n)(k_{25}C_2 - k_{52}C_5) + (z + n)(k_{34}C_3 - k_{43}C_4)] \quad (10)$$

where z is the cotransporter valence (electrical charge of the empty ion binding sites) associated with the empty carrier ($z = -2$), n is the number of Na^+ ions required for sugar transport, and F is the Faraday number. Assuming that $z = -n = -2$ and including the effect of potential, Eq. (10) then becomes Eq. (11):

$$i = 2F[C_1 k_{16}^0 \exp(-\delta\mu) - C_6 k_{61}^0 \exp(\delta\mu)]. \quad (11)$$

This equation describes the steady-state carrier-mediated current at any given membrane potential (*see* Eqs. (16)–(17)).

Experimentally, steady-state currents are being measured at ≥75 msec. Sugar-dependent currents are the difference in the current value measured at steady state before and after the addition of sugar to the bath.

Effect of Potential and Ligand Concentration

The effect of potential on Na^+ binding and dissociation reaction steps and on the empty carrier translocation is described according to the Eyring theory of reaction rates. Sugar transport may be described as a series of activated processes in which Na^+ ions and sugar move from a binding site across an energy barrier to the cytoplasmic site. Assuming the existence of a single symmetrical Eyring barrier in the membrane which is modulated by the fraction of the membrane electrical field sensed by each voltage-dependent step, the general form of the rate constants for any z and n values are given below. The rate constants with $z = -n = -2$ are shown at the right.

$$k_{12} = k_{12}^0[\mathrm{Na}]_o^n \exp(-n\alpha'\mu/2) = k_{12}^0[\mathrm{Na}]_o^2 \exp(-\alpha'\mu) \quad (12)$$

$$k_{21} = k_{21}^0 \exp(n\alpha'\mu/2) = k_{21}^0 \exp(\alpha'\mu) \quad (13)$$

$$k_{56} = k_{56}^0 \exp(-n\alpha''\mu/2) = k_{56}^0 \exp(-\alpha''\mu) \quad (14)$$

$$k_{65} = k_{65}^0[\mathrm{Na}]_i^n \exp(n\alpha''\mu/2) = k_{65}^0[\mathrm{Na}]_i^2 \exp(\alpha''\mu) \quad (15)$$

$$k_{16} = k_{16}^0 \exp(-z\delta\mu/2) = k_{16}^0 \exp(\delta\mu) \quad (16)$$

$$k_{61} = k_{61}^0 \exp(z\delta\mu/2) = k_{61}^0 \exp(-\delta\mu) \quad (17)$$

$$k_{25} = k_{25}^0 \exp(-(z + n)\delta\mu/2) = k_{25}^0 \quad (18)$$

$$k_{52} = k_{52}^0 \exp((z + n)\delta\mu/2) = k_{52}^0 \quad (19)$$

$$k_{34} = k_{34}^0 \exp(-(z + n)\delta\mu/2) = k_{34}^0 \quad (20)$$

$$k_{43} = k_{43}^0 \exp((z + n)\delta\mu/2) = k_{43}^0 \quad (21)$$

$$k_{23} = k_{23}^0[S]_o \quad (22)$$

$$k_{32} = k_{32}^0 \quad (23)$$

$$k_{45} = k_{45}^0 \quad (24)$$

$$k_{54} = k_{54}^0[S]_i \quad (25)$$

α and δ are phenomenological coefficients. δ represents the fractional dielectric distance over which the carrier ion binding site moves, and α' and α'' represent the fractional dielectric distance between the external and internal Na^+-binding sites and the membrane-solution interfaces such that $\alpha' + \delta + \alpha'' = 1$ (Läuger & Jauch, 1986). For CNa_2S and CNa_2 translocation rate constants (k_{34}, k_{43} and k_{25}, k_{52}), it is assumed that both the ion binding site and Na^+ ions move over the same dielectric distance δ in the membrane. The contribution from additional charge translocation in the cotransporter was assumed to be negligible (Jauch & Läuger, 1986). μ is the reduced potential FV/RT where V is the membrane potential and F, R, and T have their usual meanings.

Only the reaction steps involving the binding and dissociation of Na^+ and the translocation of the empty carrier are influence by the potential as shown in Eqs. (12)–(25). Negative membrane potentials would favor the sugar transport (counterclockwise reaction steps).

Simulations

All steady-state parameters, I-V curves, $K_{0.5}^{\alpha MDG}$, $i_{max}^{\alpha MDG}$, $K_{0.5}^{Na}$, and i_{max}^{Na}, and presteady-state currents were computer generated *simultaneously* under given *cis* and *trans* conditions with numerical values for 12 out of the 14 rate constants being assigned. Rate constants k_{27} and k_{72} describing phlorizin binding to CNa_2^+ were not included in the simulations but were given values that correspond to a K_D of 10 μM for phlorizin (Toggenburger, Kessler & Semenza, 1983; Ikeda et al., 1989; Kimmich, 1990).[5]

The electrical coefficients α' and δ were varied from 0 to 1 keeping $\alpha' + \delta + \alpha'' = 1$. To preserve microscopic reversibility (products of the clockwise and counterclockwise rate constants should be equal in the absence of any driving force), an internal checking procedure automatically calculates k_{52} and k_{54} from the values of all the other rate constants (*see* Appendix). Finally, simulations with the model were performed under any given Na^+ and sugar internal (*trans*) concentration. This was required to simulate sugar transport under conditions close to our experimental conditions since sugar-dependent currents were measured in *X. laevis* oocytes with finite $[Na]_i$ that may vary from 6 to 22 mM (Dascal, 1987). Equations for the steady-state parameters ($K_{0.5}^{\alpha MDG}$, $i_{max}^{\alpha MDG}$, $K_{0.5}^{Na}$, i_{max}^{Na}) derived under zero-*trans* and nonzero-*trans* are given in the Appendix (Eqs. (A36) to (A43)). Briefly, under zero-*trans* conditions, the equation for the carrier current (Eq. (A20)) can be rearranged as a function of either $[Na]_o$ or $[S]_o$ and $K_{0.5}$ and i_{max} are directly determined by the product of the rate constants (Eq. (A21)). Details of the equations used for the nonzero *trans* conditions are given in the Appendix.

Computer simulations of the current time course during a pulse of potential (presteady-state currents) were carried out by integrating Eqs. (1) to (6) assuming a time interval Δt = 10 to 50 μsec. The carrier presteady-state current is the sum of all voltage-dependent reaction steps (Läuger et al., 1981; Roy et al., 1991) with:

$$i(t) = -2F\{\alpha'[k_{12}C_1 - k_{21}C_2] - \delta[C_1k_{16} - C_6k_{61}] + \alpha''[C_5k_{56} - C_6k_{65}]\}. \quad (26)$$

The total membrane current was approximated as the sum of the oocyte background currents and the sugar-evoked carrier currents. Under our experimental conditions, we found that in native and in water-injected oocytes, the background currents can be modeled by an equivalent circuit composed of a series resistance (R_s) in series with a membrane resistance (R_m) and the membrane potential (E_r) both in parallel with the membrane capacitance (C_m) according to:

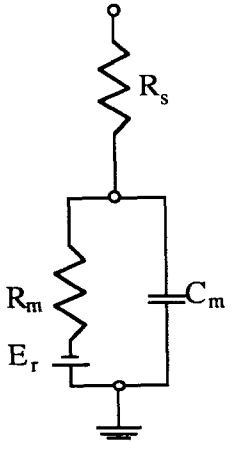

[5] Phlorizin binding to the carrier forms an inactive complex CNa_2Pz' in the presence of $[Na]_o$. According to our model, the reported voltage dependence (Aronson, 1978) is secondary to the voltage dependence of C' translocation and to Na^+ binding. Experimentally, the effect of phlorizin was to reversibly eliminate presteady-state currents and sugar-dependent currents.

where R_s is a "lump factor" that represents the sum of all possible series resistance encountered with the two-electrode voltage-clamp method. Background currents were added to the sugar-evoked carrier currents. Carrier states were considered to be in a steady state at the holding potential (e.g., −50 mV) prior to the test pulse.

As a first approximation and in the absence of any "close" initial guess, iterative simulations were preferred to a global fitting procedure. Because of the complexity of the current equation, we did not try to fit individual rate constants.

Simulations were performed until one set of rate constants was found that can globally explain our results rather than aiming at perfect multiple solutions that can account for only one result each. In addition, we did not attempt to find all possible solutions and there may be other possible solutions. For each simulation, (i) the current time course during a potential pulse in the absence and in the presence of sugar, (ii) the steady-state current-voltage relationship, and (iii) the variation of $K_{0.5}^{sugar}$, i_{max}^{sugar}, $K_{0.5}^{Na}$, i_{max}^{Na} as a function of applied voltage and of external cosubstrate concentration were generated simultaneously. In the initial simulations, we employed carrier translocation rate constants $\ll 1$ sec^{-1} and Na^+ and sugar binding and dissociation rate constants $>100{,}000$ sec^{-1} $mole^{-2}$ or sec^{-1} $mole^{-1}$. More than 2,000 simulations were then performed during which translocation rate constants were progressively increased and most association/dissociation rate constants were decreased to account for our experimental results. Optimization of the computer-generated simulations were accomplished by progressively correcting each rate constant in order to reflect the experimental results. Numerical values for each rate constant are presented, and the range for each rate constant is discussed.

Results and Discussion

Na^+/Glucose Transport Rate Constants

Computer-generated simulations were performed with the ordered kinetic model described in Fig. 1. Figure 2 shows a set of rate constants that account for the global electrical properties of the Na^+/glucose cotransporter: i.e., (i) the external Na^+, the external sugar and the voltage modulation of presteady-state currents, (ii) the sigmoidal shape of sugar-specific current-voltage relationships, and (iii) the voltage dependence of $K_{0.5}^{\alpha MDG}$, $i_{max}^{\alpha MDG}$, $K_{0.5}^{Na}$, and i_{max}^{Na} (*see* Figs. 3-9). The experimental results were found to be best described with $\delta = 0.7$, $a' = 0.3$, and $\alpha'' = 0$. The $\alpha'' = 0$ predicts an absence of voltage dependence for internal Na^+ binding, and thus asymmetrical Na^+ binding sites at the external and internal face of the membrane. Negative membrane potentials would favor the sugar transport (counterclockwise reaction steps).

Model Prediction of the Time Course of Carrier Currents

Current traces of cRNA-injected oocytes recorded in the presence of 100 mM $[Na]_o$ reach a steady state much slower than current traces of water-injected oocytes (Fig. 1, Parent et al., 1991*a*). These ON and OFF transients, distinct from the oocyte-capacitive transient, were identified as carrier presteady-state currents or carrier-gating currents. Carrier presteady-state currents were shown to be voltage dependent. They were activated by membrane depolarization from a negative holding potential. In addition, carrier presteady-state currents were not observed experimentally in the absence of $[Na]_o$ or after the addition of either sugar or phlorizin to a Na^+-rich extracellular medium.

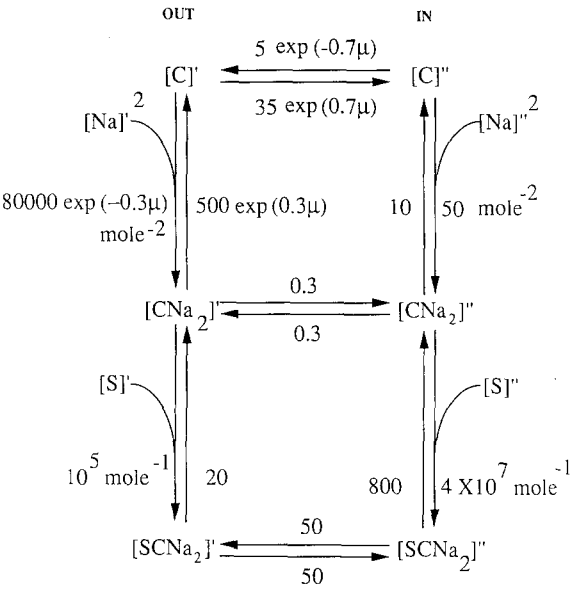

Fig. 2. Rate constants of the Na^+/glucose cotransport kinetic model that explain our results (*see* Figs. 3–7). The numerical values were found using "iterative" numerical simulations of the model (Fig. 1). Units of the rate constants are either sec^{-1}, sec^{-1} $mole^{-1}$ or sec^{-1} $mole^{-2}$.

Figure 3 shows the current traces obtained from an experiment (dots) performed with 100 mM $[Na]_o$ and the current traces predicted (solid lines) with the rate constants presented in Fig. 2. The current time course simulations were performed using the oocyte-equivalent circuit with a pulse protocol identical to the one used experimentally from a holding potential of −50 mV to test potentials from −150 to +50 mV. As seen previously, actual current traces recorded at +50 mV were described by a sum of two exponential time constants of 1 and 13 msec*. Likewise, the time course of the current traces simulated at +50 mV can be described by two time con-

* The 1-msec time constant was identified as the oocyte-capacitive transient which was not compensated under our experimental conditions. The additional time constant of 13 msec is associated with the carrier presteady-state currents.

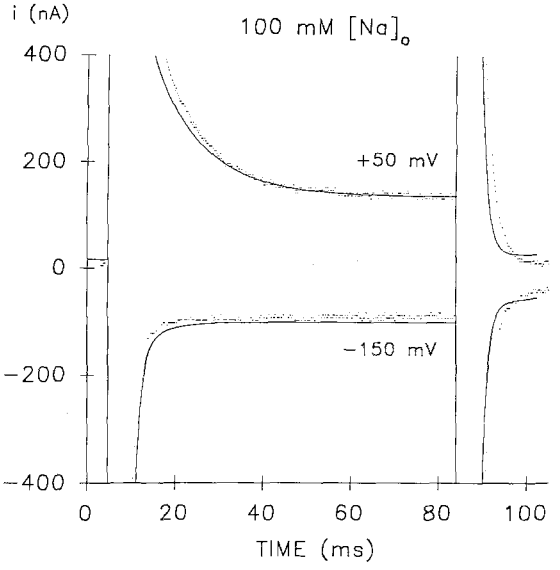

Fig. 3. Model simulation of the current time course with 100 mM $[Na]_o$. Current traces simulated in 100 mM $[Na]_o$ for $V_m = -150$ and $+50$ mV with the rate constant values shown in Fig. 2 (solid lines) were superimposed upon actual current traces (dots). The holding potential is -50 mV, and at time $t = 4.75$ msec, the potential was stepped for 80 msec to the test potential. Rate constants are shown in Fig. 2 but k_{61} was reduced from 5 to 3 sec^{-1}. The electrical circuit of the oocyte under voltage clamp is shown in the text with $R_s = 5$ kΩ, $R_m = 1.2$ MΩ, $C_m = 350$ nF, and $E_r = -65$ mV. Both the oocyte-capacitive transient ($\tau = 1$ msec) and the presteady-state carrier currents are simulated. Simulated presteady-state currents relaxed with a time constant of ≈15 msec when the membrane is pulsed from -50 to $+50$ mV, whereas there is no observable relaxation when the membrane is pulsed from -50 to -150 mV. In addition, the model accounts for the tail (OFF) currents when the potential is stepped back to -50 mV at 80 msec. In this figure and in Figs. 4 and 5, the data were obtained during the same experiment shown in Figs. 1 and 2 (Parent et al., 1991*a*), and simulations were performed with $[Na]_i = 20$ mM, $[\alpha MDG]_i = 10$ μM and a cotransporter density (C_T) of 6×10^{10} per oocyte.

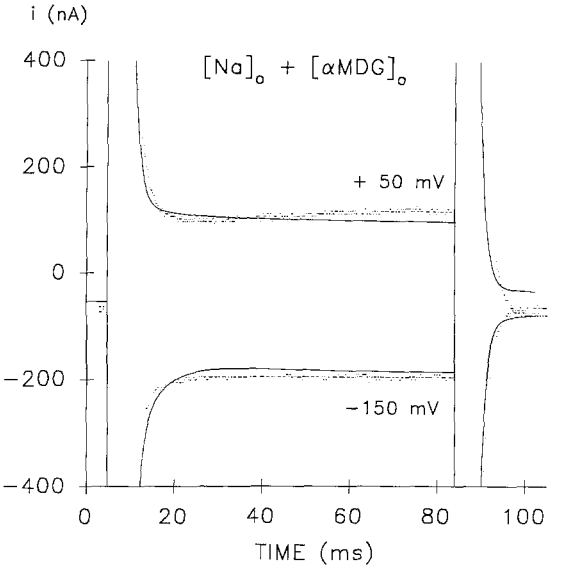

Fig. 4. Model simulation of current time course with 100 mM $[Na]_o$ and 1 mM $[\alpha MDG]_o$. Current traces simulated with 100 mM $[Na]_o$ and 1 mM $[\alpha MDG]_o$ at $V_m = -150$ and $+50$ mV (solid lines) were superimposed to actual data (dots). Same conditions as in Fig. 3. The transport model replicates the experimental observation about the absence of presteady-state currents in the presence of high $[Na]_o$ and $[\alpha MDG]_o$. Note that the steady-state carrier-mediated current measured at 75 msec is well predicted by the model (*see* Fig. 5).

stants of 1 and 13 msec. At -150 mV, current traces reach steady state with a single exponential time constant of 1 msec which is also what was observed experimentally. Tail currents measured when the potential is stepped back to the holding potential of -50 mV are also well predicted by the model. The solution of our model, therefore, mimics the ON and OFF presteady-state transient currents.

Figure 4 shows the current traces obtained in the same experiment after the addition of 1 mM $[\alpha MDG]_o$ to the bath (dots) and the current traces predicted by the model (solid lines). In the presence of sugar, the model correctly predicts both the absence of the carrier presteady-state outward currents and the increase in steady-state inward currents. In the presence of sugar, the current traces relax to a steady state within the oocyte-capacitive time constant at both $+50$ and -150 mV.

The corresponding steady-state sugar-dependent *I-V* curve predicted by the model (solid line) is compared to the actual current values in Fig. 5. Both the predicted and the measured *I-V* curves are sigmoidal with a roughly linear segment between $+20$ and -60 mV and a plateau phase at more negative potentials (*see* Fig. 2, Parent et al., 1991*a*). The correspondence between the model prediction and the actual current values is particularly satisfying in the $+10$ to -150 mV range where the voltage dependence of the kinetic parameters $K_{0.5}^{\alpha MDG}$, $i_{max}^{\alpha MDG}$, $K_{0.5}^{Na}$ and i_{max}^{Na} was measured. In addition, the model correctly predicts the absence of outward currents. The predicted carrier-mediated Na^+ leak current, which corresponds to the translocation of the CNa_2 complex, is shown as a dashed line. These current values are similar to those recorded experimentally (Umbach et al., 1990; Parent et al., 1991*a*).[6]

The model, therefore, correctly accounts for the voltage dependence of the presteady-state currents

[6] Na^+-dependent carrier currents with a phlorizin K_i of 10 μM amount to 5 to 15% of the carrier current measured in the presence of sugar (Umbach et al., 1990).

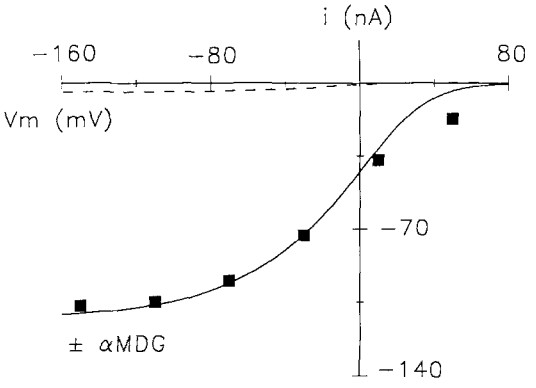

Fig. 5. Steady-state sugar-dependent *I-V* curves. Sugar-dependent *I-V* curve predicted at steady state by the model (solid line) is shown superimposed over the actual current values (±sugar) of the experiment shown in Figs. 3 and 4 (■). Simulations were performed with 100 mM $[Na]_o$, 1 mM $[\alpha MDG]_o$, 20 mM $[Na]_i$ and 10 μM $[\alpha MDG]_i$. The experiment was performed with 100 mM $[Na]_o$ and 1 mM $[\alpha MDG]_o$. The dashed line shows the predicted carrier-mediated Na^+ "leak" current in the absence of external sugar (for comparison, *see* Umbach et al., 1990).

recorded in the presence of 100 mM $[Na]_o$, the absence of presteady-state currents after the addition of sugar to the Na^+-rich medium, the magnitudes of the steady-state sugar-dependent and sugar-independent currents, and the sigmoidal shape of the sugar-dependent *I-V* curves.

Model Prediction for $K_{0.5}^{\alpha MDG}$, $K_{0.5}^{Na}$, i_{max}^{Na} and $i_{max}^{\alpha MDG}$

Steady-state kinetics of the Na^+/glucose cotransporter were reported in the experimental paper. $K_{0.5}^{\alpha MDG}$ was found to be both Na dependent and voltage dependent only at low $[Na]_o$. Figure 6*A* shows $K_{0.5}^{\alpha MDG}$ as predicted by the model (solid lines) superimposed upon experimental $K_{0.5}^{\alpha MDG}$ values (*see* Fig. 4*A*, Parent et al., 1991*a*). The model predicts qualitatively and quantitatively that the voltage dependence of $K_{0.5}^{\alpha MDG}$ increases as $[Na]_o$ is decreased from 100 to 2 mM. At 0 mV, $K_{0.5}^{\alpha MDG}$ is predicted to increase from 330 μM to 8 mM to 10 mM when $[Na]_o$ decreases from 100 to 10 to 2 mM.

$i_{max}^{\alpha MDG}$ was voltage dependent, especially between 0 and −100 mV, and slightly Na^+-dependent between 10 and 100 mM $[Na]_o$ (*see* Fig. 4*B*, Parent et al., 1991*a*). $i_{max}^{\alpha MDG}$ predicted by the model (solid lines) under the same conditions is superimposed upon the $i_{max}^{\alpha MDG}$ values that were reported for 10 and 100 mM $[\alpha MDG]_o$ (Fig. 6*B*). Our model correctly predicts the voltage dependence of $i_{max}^{\alpha MDG}$ as measured at 100 mM $[Na]_o$ over the complete range of potential and the voltage dependence of $i_{max}^{\alpha MDG}$ as measured at 10 mM $[Na]_o$ between −80 and −160 mV. Although there is some discrepancy for $i_{max}^{\alpha MDG}$ at 10 mM $[Na]_o$, especially in the −50 to 0 mV range, the transport model accounts for the weak $[Na]_o$ dependence of $i_{max}^{\alpha MDG}$ between 10 and 100 mM $[Na]_o$.

Both $K_{0.5}^{Na}$ and i_{max}^{Na} were shown to be voltage- and sugar-dependent (*see* Fig. 6, Parent et al., 1991*b*). Figure 7*A* shows $K_{0.5}^{Na}$ as predicted by the model for 1 and 20 mM $[\alpha MDG]_o$ superimposed upon the actual data. The model accounts qualitatively for the voltage dependence of $K_{0.5}^{Na}$. The predicted $K_{0.5}^{Na}$ values at 0 mV decrease from 54 to 20 mM when $[\alpha MDG]_o$ increases from 1 to 20 mM. i_{max}^{Na} simulated at 1 mM $[\alpha MDG]_o$ with the parameters of the model are shown in Fig. 7*B* superimposed upon experimental results.[7] The model accounts for the voltage dependence of i_{max}^{Na} at 1 mM $[sugar]_o$ and predicts a similar voltage dependence for i_{max}^{Na} at 20 mM $[sugar]_o$ (*results not shown*).

Presteady-State Currents

Presteady-state currents were elicited by a step of voltage from negative to positive values (Figs. 3 and 7-10, Parent et al., 1991*b*). Preasteady-state currents were modulated by $[Na]_o$, $[sugar]_o$ and membrane potential. They were specifically recorded in the absence of external sugar, and it is therefore likely that they arise from the translocation of the empty carrier in response to a positive pulse of potential. The description of the nature of the presteady-state currents relies heavily on the assumption that the empty carrier is negatively charged.[8]

Carrier presteady-state currents relaxed with a half time constant $\tau_2 \approx 13$ msec at +50 mV (*see* Figs. 3 and 8, Parent et al., 1991*a*). Given that only one relaxation was observed, a minimum of two slow steps along the transport cycle is required to describe the presteady-state currents (Hille, 1984; Wierzbicki et al., 1990; Roy, Wierzbicki & Sauré, 1991). Figure 8 shows the distribution of the six possible carrier states when the membrane potential is stepped from −50 to +50 mV and then back to −50 mV in the presence of 100 mM $[Na]_o$. In the

[7] Note that $i_{max}^{\alpha MDG}$ and i_{max}^{Na} were measured on separate experiments. Ideally, at saturating $[Na]_o$ and saturating $[\alpha MDG]_o$, $i_{max}^{\alpha MDG}$ would be equal to i_{max}^{Na} when measured on the same oocyte. In our simulations, C_T was scaled to reflect the difference in current density between the two oocytes.

[8] The following interpretation of the carrier presteady-state currents rests entirely on the assumption that the empty carrier is negatively charged ($z \neq 0$) and δ is greater than zero (presteady-state currents correspond to the gating currents). We have not tried to find a solution with $z = 0$ or with noninteger charges ($z = 1/4, 1/2$, etc.).

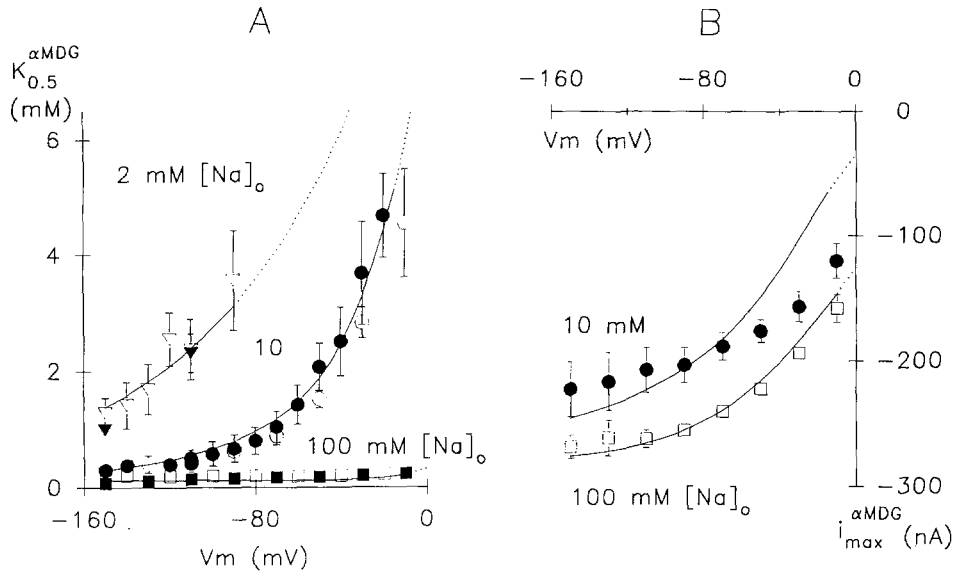

Fig. 6. Voltage and Na^+ dependence of $K_{0.5}^{\alpha MDG}$ and $i_{max}^{\alpha MDG}$. (*A*) $K_{0.5}^{\alpha MDG}$ fit to experimental data using the rate constants shown in Fig. 2. $K_{0.5}^{\alpha MDG}$ simulated with transport model (solid lines) is shown superimposed to $K_{0.5}^{\alpha MDG}$ measured experimentally with 2 (▽,▼), 10 (●,○) and 100 (□,■) mM $[Na]_o$. $K_{0.5}^{\alpha MDG}$ and $i_{max}^{\alpha MDG}$ measured at 10 (●) and 100 (□) mM $[Na]_o$ were measured on the same oocyte. The error bar represent the error on the estimation of $K_{0.5}^{\alpha MDG}$ from actual current values. $K_{0.5}^{\alpha MDG}$ simulation was performed according to Eq. (A39). The dotted lines show the model predictions beyond the experimental data. At 0 mV, $K_{0.5}^{\alpha MDG}$ would be 8 mM at 10 mM $[Na]_o$ and 10 mM at 2 mM $[Na]_o$. (*B*) $i_{max}^{\alpha MDG}$ fit to experimental data. $i_{max}^{\alpha MDG}$ simulated with transport model superimposed to $i_{max}^{\alpha MDG}$ was measured experimentally with 10 (●) and 100 mM $[Na]_o$ (□). $i_{max}^{\alpha MDG}$ simulation was performed according to Eq. (A37) with the rate constants shown in Fig. 2. C_T is 15×10^{10} carriers oocyte^{-1}.

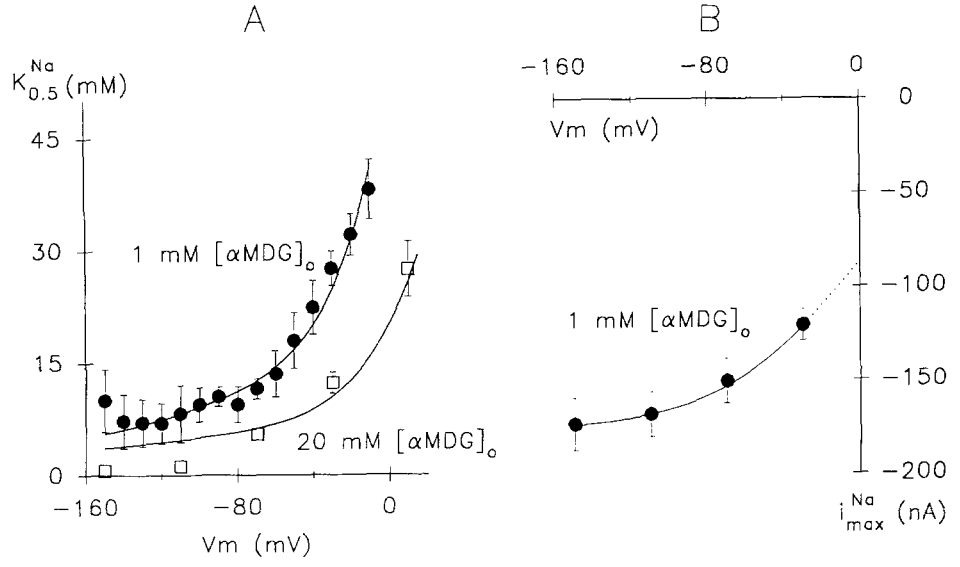

Fig. 7. Voltage and sugar dependence of $K_{0.5}^{Na}$ and i_{max}^{Na}. (*A*) $K_{0.5}^{Na}$ fit to experimental data. The error bar represents the error on the fit to the Hill equation. $K_{0.5}^{Na}$, simulated with the transport model (solid lines) are shown superimposed to $K_{0.5}^{Na}$ obtained experimentally for 1 (●) and 20 mM $[\alpha MDG]_o$ (□) in two separate experiments. $K_{0.5}^{Na}$ was simulated from Eq. (A43). (*B*) i_{max}^{Na} fit to experimental data. i_{max}^{Na} simulated with the transport (solid lines) superimposed to i_{max}^{Na} was obtained experimentally for 1 mM $[\alpha MDG]_o$. The curve shows the behavior of i_{max}^{Na} according to the rate constants shown in Fig. 2. i_{max}^{Na} was simulated from Eq. (A41). C_T is 10×10^{10} carriers oocyte^{-1}. The dotted lines show the model predictions beyond the experimental data.

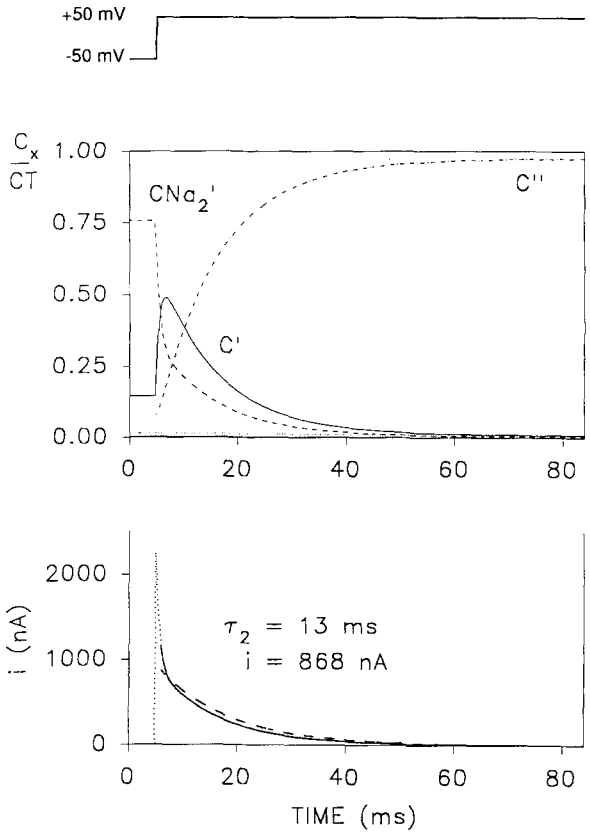

Fig. 8. Reconstruction of the carrier presteady-state current. Upper panel. Time course of carrier distribution was predicted by the model in the presence of 100 mM $[Na]_o$ when the membrane potential is stepped from −50 to +50 mV. Only three carrier states C', CNa_2' and C'' account for >95% of all carrier states throughout the simulation. At −50 mV, the major state carrier is CNa_2'. As the membrane potential rises to +50 mV, CNa_2' is converted into C' and C''. This series of reaction steps is responsible for the ON currents (*see* lower panel). Lower panel. Carrier-mediated current was reconstructed in the absence of the oocyte-capacitive transient using Eq. (26) in the presence of 100 mM $[Na]_o$. There is no steady-state carrier-mediated current at V_h = −50 mV (prior to the pulse). As the potential is stepped from −50 to +50 mV at 4.75 msec, carrier-mediated current rises rapidly to a peak at 1320 nA before vanishing at steady state. Under our experimental conditions, the rapid rise of the presteady-state current is likely to be obscured by the oocyte-capacitive transient (dotted line). The carrier presteady-state current can be fitted by a single exponential function (dashed line) $i = i_o \exp(-t/\tau)$ with t = time, τ = 13 msec and i_o = 868 nA where i_o is the maximum current extrapolated at the beginning of the pulse (4.75 msec). For this simulation, C_T was 4×10^{10} carriers oocyte^{-1}.

absence of sugar, four carrier states are mainly present; C', CNa_2', C'' and CNa_2''. As observed at the holding potential of −50 mV (prior to the onset of the pulse), 75% of the carrier is in the CNa_2' state with C' (15%) and C'' (7%) completing the carrier distribution. This represents an asymmetrical distribution of the carrier with more carriers available from the external than from the internal face of the membrane. The distribution and the translocation of C' and C'' is controlled by the membrane potential with a negative membrane potential more likely to increase the concentration of C'. Translocation of $CNa_2' \rightleftharpoons CNa_2''$ is electrically silent (Eqs. (16)–(19)). As the potential is stepped from −50 to +50 mV (at time t = 4.75 msec), CNa_2' is dissociated into external Na^+ ions and C', and then the empty carrier, returns to the internal face of the membrane (C''). At the end of the pulse, C'' represents 98% of the carrier states.[9] As a consequence of the actual rate constants at +50 mV (k_{21} = 911 sec^{-1}, k_{12} = 4.4 sec^{-1}, k_{16} = 141 sec^{-1} and k_{61} = 0.74 sec^{-1}), there is a transitory accumulation of C' during the pulse. The empty carrier concentration C' rises from 15% (at V_h = −50 mV) to peak at 45%, 2 msec after the step of potential, before vanishing at the steady state. The carrier transient current peaks at 1320 nA at the beginning of the pulse (Fig. 8, lower panel). The predicted transient current is described by a single exponential function (dashed line) with a time constant τ = 13 msec which corresponds to the observed time constant for the presteady-state current. The transient outward current can, therefore, be understood as the result of the rearrangement of three carrier states $CNa_2' \overset{k21}{\rightleftharpoons} C' \overset{k16}{\rightleftharpoons} C''$. Rate constants k_{21} and k_{16} are the two "slow" rate constants required to generate the ON rate for the presteady-state currents. The rising phase of the carrier presteady-state currents was not observed experimentally as it is obscured by the capacitive transient of the oocyte. The OFF presteady-state current simulated as the potential is stepped back to −50 mV is also shown. The OFF rate is controlled by the value of the rate constant k_{61} in the reaction $C' \overset{k61}{\rightleftharpoons} C''$.

The two-step carrier rearrangement from −50 to +50 mV can also explain the increase of presteady-state currents with increasingly negative holding potentials, e.g., current increasing as the holding potential was made more negative (*see* Fig. 9, Parent et al., 1991*a*). Simulations with the model indeed predicts that increasing the holding potential from −50 to −200 mV before the test potential of +50 mV will also increase from 75 to 97% the number of carriers in the CNa_2' state. So when the potential is stepped to +50 mV, the transient increase in C' and the carrier-mediated currents are accordingly larger.

[9] The backward reaction $C' \overset{k61}{\leftarrow} C''$ is not favored by positive potentials. At +50 mV, the rate constant k_{61} is only 0.74 sec^{-1}. In addition, with $K_{Na''}$ between 44 and 450 mM, there is no predicted accumulation of CNa_2'' species for $[Na]_i$ below 40 mM.

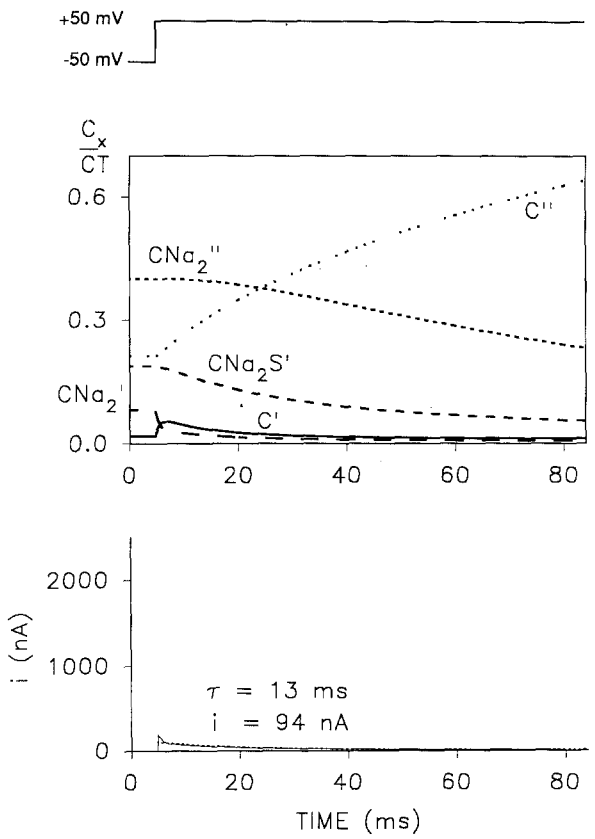

Fig. 9. Reconstruction of the carrier presteady-state current in the presence of sugar. Upper panel. Time course of carrier distribution was predicted by the model in the presence of 100 mM $[Na]_o$ and 1 mM $[\alpha MDG]_o$ from −50 to +50 mV. The three major carrier states are CNa_2'' (40%), CNa_2S' (20%) and C'' (21%) at −50 mV. As the potential is stepped to +50 mV, C'' rises steadily to 63% as positive membrane potential favors the accumulation of empty carriers at the internal face. Lower panel. Carrier-mediated current is reconstructed in the absence of the oocyte-capacitive transient using Eq. (11) in the presence of 100 mM $[Na]_o$ and 1 mM $[\alpha MDG]_o$. Note this time, the steady-state current of −50 nA measured at V_h = −50 mV. When the potential is stepped from −50 to +50 mV, carrier-mediated current transiently rises only to 88 nA, before reaching a steady-state value of +12 nA. Current relaxation was approximated by one exponential function with i_1 = 94 nA and τ_1 = 13 msec (dashed line). The presteady-state current generated under these conditions is 10-fold smaller than in the absence of $[Na]_o$ but the current relaxes with the same time constant τ of 13 msec (*see* Fig. 8). As in Fig. 8, C_T is 4 × 10^{10} carriers oocyte^{-1}.

We reported that presteady-state currents were not observed after the addition of sugar to the Na-rich medium (*see* Fig. 7*C*, Parent et al., 1991*a*). Figure 9 presents the distribution profile of the carrier states simulated with 100 mM $[Na]_o$ and 1 mM $[\alpha MDG]_o$ during a pulse of potential from −50 to +50 mV. At −50 mV and in the presence of $[Na]_o$ and $[sugar]_o$, the major carrier states are CNa_2'' (40%), CNa_2S' (20%) and C'' (21%) (Fig. 9, upper panel). The virtual absence of CNa_2S'' is due to the rapid dissociation (k_{45} = 800 sec^{-1}) into CNa_2'' and internal free sugar. CNa_2' and C' are only 8 and 2% of the carriers present. As result, when the potential is stepped from −50 to +50 mV, the clockwise reaction $CNa_2' \overset{k21}{\rightarrow} C' \overset{k16}{\rightarrow} C''$ is negligible. Our model predicts that carrier-mediated current transiently rises only to 94 nA, but relaxes to a steady current of +12 nA with a time constant τ of 13 msec (Fig. 9, lower panel). Presteady-state currents generated in the presence of saturating $[\alpha MDG]_o$ are thus 10-fold smaller than the presteady-state currents predicted solely in the presence of 100 mM $[Na]_o$. We think that the modest peak current and the noncompensated capacitive transient account for our failure to detect experimentally presteady-state currents under these conditions. As the potential is stepped back to −50 mV, an inward current developes that relaxes slowly back to −45 nA.

Finally, presteady-state currents were not observed in low external Na^+ and $[\alpha MDG]_o$ (*see* Fig. 7*D*, Parent et al., 1991*a*). Simulations performed with 10 mM $[Na]_o$ show that at the holding potential of −50 mV only 3% of all carriers are in the CNa_2' state compared to 75% in the presence of 100 mM $[Na]_o$. Under these conditions, k_{12} is only 15 sec^{-1} as compared to 1458 sec^{-1} in the presence of 100 mM $[Na]_o$. Free carriers are still preferentially distributed at the external surface (C' = 66%) at −50 mV, and as the potential is pulsed to +50 mV, C' is transformed to C'' mono-exponentially with a time constant τ of 4 msec. Again, this rapid decay of C' to C'' is likely to be masked experimentally by the oocyte-capacitive transient.

The time course of the carrier-mediated currents as predicted by our model has been reconstructed at −150 and +50 mV in the absence of the oocyte-capacitive transient (Fig. 10). The time course of the predicted carrier-mediated current with 100 mM $[Na]_o$ is shown as a solid line. The carrier-mediated current predicted after the addition of 1 mM $[\alpha MDG]_o$ is shown as a dashed line. There is a significant transient carrier-mediated current only in the presence of 100 mM $[Na]_o$ and at +50 mV ($\tau \approx$ 13 msec). This current vanishes well before the steady-state electrical properties of the cotransporter were measured (at ≈75 msec). In contrast, there is a significant steady-state inward current at −150 mV as predicted after the addition of $[\alpha MDG]_o$. The difference in the carrier-mediated current measured at steady state before (solid line) and after (dashed line) the addition of sugar to the bath is the sugar-dependent current. The model predicts that sugar-dependent currents measured at steady state will be negligible or close to zero at +50 mV and will increase as the membrane potential is made more negative (*see* Fig. 5).

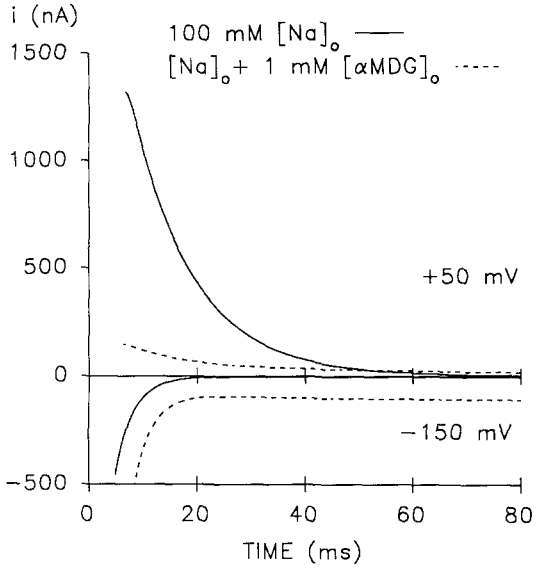

Fig. 10. Time course of the carrier-mediated current as predicted with the model. Carrier-mediated current is reconstructed in the absence of the oocyte-capacitive transient using Eq. (26) in the presence of 100 mM $[Na]_o$ (solid line) and after the addition of 1 mM $[\alpha MDG]_o$ to the bath (dashed line). Carrier-mediated current is shown as predicted at the test potential of +50 mV (upper panel) and −150 mV (lower panel). Presteady-state current peaks at 1320 nA at 6.75 msec in the presence of 100 mM $[Na]_o$ only. Sugar-dependent currents are the difference in current measured at 75 msec before and after the addition of sugar to the bath. At −150 mV, sugar-dependent currents are −105 nA. C_T was 6×10^{10} carriers oocyte^{-1}.

Evaluation of the Model Rate Constants

The preceding description clearly illustrates how the characteristics of the presteady-state currents set strong limitations in the values of at least five rate constants k_{12}, k_{21}, k_{16}, k_{61} and k_{32}. Presteady-state currents can only be observed significantly over the oocyte-capacitive transient providing that CNa_2' relaxes to C'' with $CNa_2' \overset{k21}{\rightarrow} C' \overset{k16}{\rightarrow} C''$ at +50 mV. The relaxation time constant of the presteady-state current is determined largely by k_{16} ($C' \overset{k16}{\rightarrow} C''$). Increasing k_{16}^0 from 35 to only 70 sec^{-1} would accelerate the relaxation of presteady-state currents up to the value of the oocyte-capacitive transient. The magnitude of the carrier peak transient current is controlled by the concentration of carrier state CNa_2' and C' before the depolarization pulse at any given C_T. Off-current or tail presteady-state currents are determined by k_{61} in the reverse reaction $C' \overset{k61}{\leftarrow} C''$. The $[Na]_o$ dependence of the presteady-state currents requires that $k_{12}^*[Na]_o$† must be such that at a holding potential of −50 mV and in the absence of external sugar, CNa_2' would be the major carrier state with 100 mM $[Na]_o$ but not with 10 mM $[Na]_o$. Our failure to observe presteady-state currents in low external Na^+ ions ($[Na]_o < 30$ mM) sets an upper limit on k_{12} ($k_{12} \ll 4 \times 10^5$). When k_{12} is increased beyond this limit, one may artificially generate "presteady-state currents" at any finite $[Na]_o$. Finally, the absence of detectable presteady-state currents in the presence of external sugar indicates that rate constant k_{32} must be lower than 25 sec^{-1} so that the fully loaded carrier CNa_2S' cannot reverse to $CNa_2' \overset{k21}{\rightarrow} C' \overset{k16}{\rightarrow} C''$. Simulations have shown that the magnitude of the predicted presteady-state currents decreases progressively as k_{32} is reduced from 20 to 1 sec^{-1} in the presence of 1 mM $[\alpha MDG]_o$. It is concluded that the absolute values, and not only the ratio of these five rate constants, directly modulate presteady-state currents. Considering the requirement for external Na^+- and sugar-association rate constants (k_{12}, k_{21}, k_{32}) and carrier-translocation rate constants (k_{16} and k_{61}), it is difficult to conceive that the carrier-mediated sugar transport can be described as a true rapid equilibrium system.

The voltage dependence of steady-state electrical properties $K_{0.5}$ and i_{max} is empirically described by the coefficients α' and δ, respectively.[10] The fractional electrical coefficient for external Na^+ binding, α', characterizes the voltage dependence of $K_{0.5}$, and the fractional electrical coefficient for the carrier translocation, δ, characterizes the voltage dependence of i_{max}. As seen in the companion paper, both $K_{0.5}^{Na}$ and $K_{0.5}^{\alpha MDG}$, at low external $[Na]_o$, are voltage dependent. Their voltage dependence is best described by α' values between 0.25 and 0.35. Increasing α' beyond this range would steepen the voltage dependence of $K_{0.5}^{\alpha MDG}$ and $K_{0.5}^{Na}$. Voltage coefficient δ controls the sigmoidal shape of the *I-V* relationships and the Na dependence of $i_{max}^{\alpha MDG}$. Only δ values ≥ 0.7 can account for the sigmoidal shape and the Na dependence of $i_{max}^{\alpha MDG}$ curves. Smaller δ values tend to give *I-V* curves that are linear over the complete range of potential and larger external Na dependence than experimentally measured. The voltage dependence of i_{max}^{Na} can be accounted for by δ values ranging from 0.4 to 0.8. Since by definition $\alpha' + \delta + \alpha'' = 1$, this leaves the coefficient α'' close to zero, suggesting a quasi-absence of voltage dependence for internal Na^+ binding. Experiments from the internal face of the membrane are now required to determine the value of α'' and to examine the voltage dependence of internal Na^+ binding.

† Rate constant k_{ij}^* includes the effect of potential on the rate constant but not the effect of concentrations. See Appendix for further details.

[10] The interpretation of the presteady-state currents relies on the assumption that the empty carrier is negatively charged but the model can still qualitatively account for the voltage dependence of $K_{0.5}^{\alpha MDG}$, $K_{0.5}^{Na}$, i_{max}^{Na}, and $i_{max}^{\alpha MDG}$ in the case where z is positive or equal to zero.

The Na^+-dependence of $K_{0.5}^{\alpha MDG}$ and $i_{max}^{\alpha MDG}$ is a function of the rate constants k_{21} and k_{12} (whose ratio would be equivalent to KNa'). KNa' values between 50 and 100 mM were found compatible with the experimental $K_{0.5}^{Na}$ values extrapolated at 0 mV. However, we found that increasing k_{12}, k_{21}, k_{32}, k_{23}, k_{56}, k_{65}, and k_{45} by a factor of 10 (thus conserving the same apparent KNa', KNa", and KNaS' values), would overestimate the Na^+ dependence of $K_{0.5}^{\alpha MDG}$ and reduce all the $K_{0.5}^{Na}$ values. This further suggests that k_{21} and k_{12} cannot be replaced by their equilibrium constant.

Rate constants k_{34} and k_{43} describe the membrane translocation of the fully loaded carrier $CNa_2S' \rightleftharpoons CNa_2S''$. In our model, k_{43} can be given any value between 0.1 and 1000 sec^{-1} without affecting the presteady-state currents and the cotransporter steady-state kinetics $K_{0.5}^{\alpha MDG}$, $K_{0.5}^{Na}$, $i_{max}^{\alpha MDG}$ and i_{max}^{Na}. In contrast, k_{34} is only acceptable in a narrow range between 35 and 100 sec^{-1}. Decreasing k_{34} below 35 sec^{-1} would overestimate $K_{0.5}^{\alpha MDG}$ and $K_{0.5}^{Na}$ while underestimating the current.[11] Increasing k_{34} above 100 sec^{-1} would steepens the dependence of $i_{max}^{\alpha MDG}$ and i_{max}^{Na} on membrane potential and significantly underestimate $K_{0.5}^{\alpha MDG}$ at low $[Na]_o$ and $K_{0.5}^{Na}$. In the 35- to 100-sec^{-1} range, the variations of the steady-state parameters predicted by the model are within the error associated with the experimental results. Interestingly, the translocation rate constant of the loaded carrier (k_{34}) agrees with the Na^+/glucose cotransporter turnover rates reported from 5 to 70 sec^{-1} (*see* Peerce & Wright, 1984; Schultz, 1986).

The carrier-mediated Na^+ leak current, $CNa_2' \leftrightharpoons CNa_2''$ translocation in the absence of sugar, is required to account for the observation of steady-state Na^+-dependent and phlorizin-inhibited currents (Umbach et al., 1990; Parent et al., 1991*a*). The magnitude of the carrier "Na^+ leakage" current is most sensitive to rate constants k_{25} and k_{52}. Increasing k_{25} and k_{52} increases the proportion of sugar-independent over sugar-dependent current. One should note, however, that the carrier Na^+ leak current is not required to account for the presteady-state currents or to account for the carrier kinetics. Rate constants k_{25} and k_{52} can be set to 0.0 sec^{-1} without affecting the adequateness of the model to $K_{0.5}^{\alpha MDG}$, $i_{max}^{\alpha MDG}$, $K_{0.5}^{Na}$, and i_{max}^{Na} or the characteristics of the presteady-state currents (*results not shown*).

Rate constants k_{56} and k_{65} in $C'' \rightleftharpoons CNa_2''$ give the apparent internal Na dissociation constant KNa". At any given k_{65}, increasing k_{56} from 1 to 50 sec^{-1} will increase the current and steepen the voltage dependence of i_{max}^{Na} and $i_{max}^{\alpha MDG}$ so k_{56} can be set within a definite range. Rate constant k_{65} can be set anywhere between 20 and 1000 sec^{-1} without any significant effect on $K_{0.5}^{\alpha MDG}$, $K_{0.5}^{Na}$, $i_{max}^{\alpha MDG}$, i_{max}^{Na} predicted under zero-*trans* conditions. However, the range of *trans*-sugar inhibition effect is most sensitive to k_{65}. In the absence of experimental results performed under controlled *trans* conditions, k_{65} is yet to be narrowed down.

Dissociation constants for Na^+ ions and sugar were computed. The external Na^+ ions dissociation constant KNa' (KNa' = k_{21}/k_{12}) is 79 mM at 0 mV and decreases to 24 mM as the membrane potential increases to −150 mV. The Na^+ dissociation constant from the internal face (KNa") is given by the ratio of the constants k_{56}/k_{65}. In the absence of a direct experimental result, any value of KNa" between 40 and 1000 mM seems compatible with our results. The actual value may be inferred in the future from experiments measuring the Na-*trans* (Na_i) effect on sugar transport in *Xenopus* oocytes. The external sugar dissociation constant KNa_2S' is 200 μM. Again, in the absence of direct experimental evidence, our results are compatible with any value of KNa_2S'' between 100 μM and 5 mM.

Model Predictions on *TRANS* Effects

Na-*Trans* Inhibition on the Cotransporter Sugar-Dependent Current

Trans or internal Na^+ ions inhibit sugar influx in BBMVs (*see* for instance, Kessler & Semenza, 1983; Kaunitz & Wright, 1984; Supplisson, 1988). In our model, the internal Na^+ dissociation constant corresponds approximately to the half-maximum for Na-*trans* inhibition (K_i^{Na}) on the sugar-dependent currents. KNa" values from 40 to 400 mM are compatible with our results with the maximum Na-*trans* inhibition effect at the lower end of the spectrum. With KNa" = 44 mM, simulations shows that increasing $[Na]_i$ from 0 to 500 mM (in the absence of internal sugar) would progressively inhibit sugar-dependent currents (Fig. 11). Negative inside potential ($V_m < 0$ mV) would relieve Na-*trans* inhibition as reported by Kimmich and Randles (1988) in chicken enterocytes. With KNa" = 44 mM, our model predicts a K_i for Na-*trans* inhibition of 44 mM at 0 mV, of 75 mM at −50 mV and of 350 mM at −150 mV. Our predicted K_i values agree with the K_i value of 54 mM reported at 0 mV by Kaunitz and Wright (1984).

[11] Any increase in the limiting rate constant of the cycle leads to an increase in the carrier-mediated current.

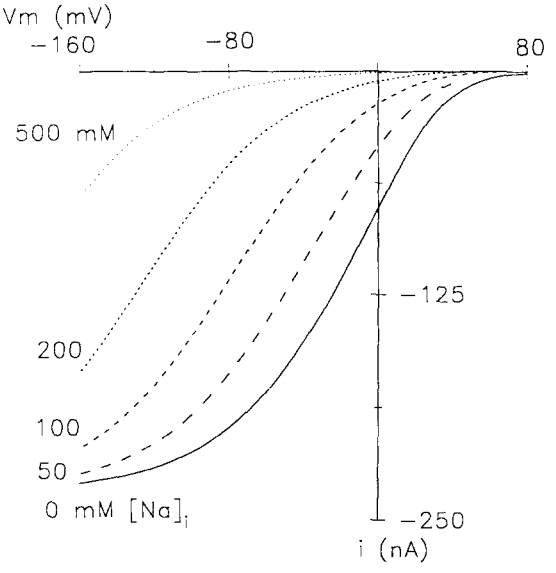

Fig. 11. *Trans*-Na inhibition on sugar-dependent currents as predicted by the model. Sugar-dependent *I-V* curves were simulated with 100 mM $[Na]_o$ and 1 mM $[\alpha MDG]_o$. Internal sugar was fixed at 0 μM. *Trans*-Na was varied between 0 and 500 mM. KNa″ = 44 mM, k_{65} = 5000 sec^{-1} and k_{56} = 10 sec^{-1}. C_T is 2 × 10^{11} carriers oocyte^{-1}.

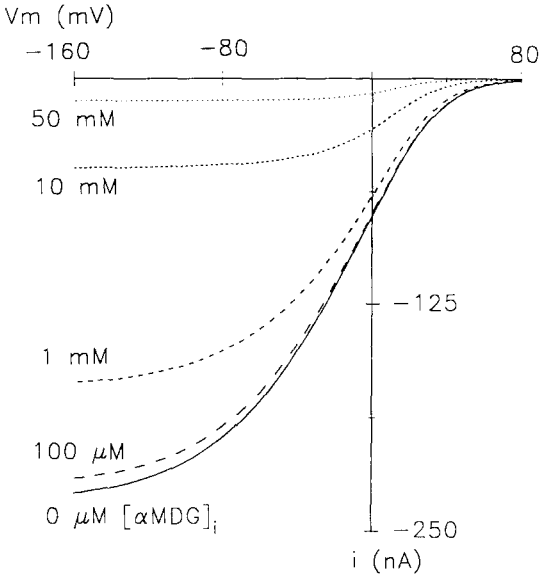

Fig. 12. *Trans*-sugar inhibition on sugar-dependent currents as predicted by the model. Sugar-dependent *I-V* curves were simulated with 100 mM $[Na]_o$ and 1 mM $[\alpha MDG]_o$. Internal $[Na]_i$ was kept at 0 mM. *Trans*-sugar was varied from 0 to 50 mM. KNaS″ = 4 mM, KNa′ = 44 mM, k_{65} = 5000 sec^{-1} and k_{56} = 10 sec^{-1}. C_T is 2 × 10^{11} carriers oocyte^{-1}.

Sugar-*Trans* Inhibition on the Cotransporter Sugar-Dependent Currents

Our model also predicts that *trans* sugar will inhibit sugar-dependent currents measured in the presence of external (*cis*) Na^+ and sugar. The predicted midpoint of internal *trans*-sugar inhibition on currents is dependent upon the value attributed to KNa″. With KNa″ = 44 mM, increasing internal sugar from 0 to 50 mM decreases sugar-dependent currents and membrane potential is not predicted to relieve the sugar-*trans* effect (Fig. 12). In our model, the magnitude of the *trans*-sugar effect is of course related to KNa″. Increasing KNa″ toward the upper end of the spectrum would decrease the K_i for *trans*-sugar inhibition.[12] With KNa″ = 450 mM and KNaS″ = 200 μM, the major inhibition effect is found in the 50- to 500-μM range. Decreasing k_{65} to 5000 sec^{-1}, therefore decreasing KNa″ to 44 mM and KNaS″ to 4 mM, increases the midpoint of internal *trans*-sugar inhibition to 4 mM. Sugar-*trans* inhibition effect is predicted in the absence and in the presence of internal Na (no Na-*trans* relief effect). In addition, increasing $[S]_i$ above the value of KNaS″ is predicted to cause an increase in $K_{0.5}^{\alpha MDG}$ at low $[Na]_o$ in the −50 to 0-mV range (*results not shown*). Kessler and Semenza (1983) have demonstrated sugar-*trans* inhibition in BBMV uptake experiments.

[12] At fixed k_{56} = 10 sec^{-1}, increasing k_{65} from 50 to 5000 sec^{-1} mol^{-2} decreases KNa″ and increases KNaS″. In the absence of any result obtained under controlled *trans* conditions, KNa″ was giving values between 40 and 450 mM. KNaS″ varied accordingly from 4 mM to 200 μM.

Conclusion

A 6-state ordered ($2Na^+ : S$) kinetic model was found to account for the presteady-state currents and the steady-state electrical properties of the Na^+/glucose cotransporter. Our results are compatible with a negatively charged carrier with two Na^+ binding sites located within the membrane electrical field (α' = 25 to 35%). The Na^+ ion binding sites on the empty carrier traverses 80 to 60% of the membrane electrical field during translocation. Negative membrane potential facilitates sugar transport. The preferential accumulation of the empty carrier at the outer membrane requires that the membrane potential be equal or more negative than −35 mV.

Presteady-state currents are described as gating currents of the Na^+/glucose cotransporter. They are accounted for by the reaction steps $CNa_2' \overset{k_{21}}{\underset{}{}} C' \overset{k_{16}}{\underset{}{}} C''$ when the membrane potential is stepped from −50 to +50 mV in the presence of saturating $[Na]_o$. The relaxation time constant is function of both k_{21} and k_{16}, and the magnitude of the current is deter-

mined by the proportion of CNa_2' species available before the potential is stepped to +50 mV. Both ON and OFF currents are crucial in limiting the rate constants k_{12}, k_{21}, k_{16}, k_{61} and k_{32}. In our model, that means k_{21} should be between 200 and 600 sec^{-1}, k_{16} between 25 and 55 sec^{-1}, k_{61} between 3 and 5 sec^{-1} and k_{32} between 1 and 30 sec^{-1}. Because of the presteady-state characteristics, k_{21} and k_{12} cannot be replaced by the equilibrium constant for external Na^+ ions binding KNa', and k_{32}, and k_{23} cannot be replaced by the equilibrium constant for external sugar $KNaS'$ which suggests that the rapid equilibrium assumption is improper in our conditions.

Rate-limiting steps for sugar transport are dependent upon the membrane potential and upon $[Na]_o$ and $[sugar]_o$. Under saturating $[Na]_o$ and $[S]_o$, the rate limiting for sugar transport is the outward carrier translocation $C' \overset{k61}{\leftarrow} C'$ at any membrane potential more positive than −43 mV. In the membrane potential range between −43 and −134 mV, the rate-limiting step becomes the internal Na^+ ions dissociation rate constant k_{56}. Since rapid equilibrium was not assumed in our model, k_{12} may be rate limiting at very low $[Na]_o$ (<10 mM) at negative membrane potential between −134 and 0 mV simply because the effect of membrane potential is stronger on k_{61} than on k_{12}.

The ratio of the empty carrier translocation $k_{16}/k_{61} = 7$, the ratio of the loaded carrier translocation $k_{34}/k_{43} = 1$, and the ratio of the loaded carrier translocation over the empty carrier translocation $k_{34}/k_{61} = 10$. This agrees with previous reports that J_{max} for the Na^+/glucose cotransporter measured in BBMV under equilibrium exchange condition ($[Na]_o = [Na]_i$ and $[S]_o = [S]_i$) would be 5 to 10 times bigger than J_{max} measured under zero-*trans* conditions (*see* Stevens, Kaunitz & Wright, 1984).

The Na^+/glucose cotransporter model is functionally asymmetrical with asymmetry in the rate constants for empty carrier translocation ($k_{61}^0 > k_{16}^0$), an absence of voltage dependence for internal Na^+ binding ($\alpha'' = 0$), and internal Na^+ binding rate constant k_{65}^0 200- to 2000-fold smaller than external Na^+ binding k_{12}^0 ($KNa' = 80$ mM and $KNa'' = 44$ mM).

We are grateful to Drs. A. Berteloot, S. Ciani, and J.-Y. Lapointe for stimulating discussions and thank our colleagues for comments. L.P. was recipient of a post-doctoral fellowship from the Medical Research Council of Canada. This work was supported by a grant from the U.S. Public Health Service DK 19567.

References

Aronson, P.S. 1978. Energy-dependence of phlorizin binding to isolated renal microvillus membranes. *J. Membrane Biol.* **42:**81–98

Dascal, N. 1987. The use of *Xenopus* oocytes for the study of ion channels. *CRC Crit. Rev. Biochem.* **22:**317–837

Goldner, A.M., Schultz, S.G., Curran, P.F. 1969. Sodium and sugar fluxes across the mucosal border of rabbit ileum. *J. Gen. Physiol.* **53:**362–383

Hille, B. 1984. Ion Channels of Excitable Membranes. Sinauer, Sunderland (MA)

Hopfer, U., Groseclose, R. 1980. The mechanism of Na^+-dependent D-glucose transport. *J. Biol. Chem.* **255:**4453–4462

Ikeda, T.S., Hwang, E.-S., Coady, M.J., Hirayama, B.A., Hediger, M.A., Wright, E.M. 1989. Characterization of a Na^+/glucose cotransporter cloned from rabbit small intestine. *J. Membrane Biol.* **110:**87–95

Jauch, P., Läuger, P. 1986. Electrogenic properties of the sodium-alanine cotransporter in pancreatic acinar cells: II. Comparison with transport models. *J. Membrane Biol.* **94:**117–127

Kaunitz, J.D., Wright, E.M. 1984. Kinetics of sodium D-glucose cotransport in bovine intestinal brush border vesicles. *J. Membrane Biol.* **79:**41–51

Kessler, M., Semenza, G. 1983. The small-intestinal Na^+ D-glucose cotransporter: An asymmetric gated channel (or pore) responsive to $\Delta\psi$. *J. Membrane Biol.* **76:**27–56

Kimmich, G.A. 1990. Membrane potentials and the mechanism of intestinal Na^+-dependent sugar transport. *J. Membrane Biol.* **114:**1–27

Kimmich, G.A., Randles, J. 1988. Na^+-coupled sugar transport: Membrane potential-dependent K_m and K_i for Na^+. *Am. J. Physiol.* **255:**C486–C494

King, E.L., Altman, C. 1956. A schematic method of deriving the rate laws for enzyme-catalyzed reactions. *J. Phys. Chem.* **60:**1375–1378

Lapointe, J.-Y., Hudson, R.L., Schultz, S.G. 1986. Current-voltage relations of sodium-coupled sugar transport across the apical membrane of *Necturus* small intestine. *J. Membrane Biol.* **93:**205–219

Läuger, P., Benz, R., Stark, G., Bamberg, E., Jordan, P.C., Fahr, A., Brock, W. 1981. Relaxation studies of ion transport systems in lipid bilayer membranes. *Q. Rev. Biophys.* **14:**513–598

Läuger, P., Jauch, P. 1986. Microscopic description of voltage effects on ion-driven cotransport systems. *J. Membrane Biol.* **91:**275–284

Parent, L., Supplisson, S., Loo, D.D.F., Wright, E.M. 1991*a*. Electrogenic properties of the cloned Na^+/glucose cotransporter: I. Voltage-clamp studies. *J. Membrane Biol.* **125:**49–62

Parent, L., Supplisson, S., Loo, D.D.F., Wright, E.M. 1991*b*. Electrogenic properties of the cloned Na^+/glucose transporter: Transport model under non rapid equilibrium conditions. *Biophys. J.* **59:**396 (Abstr.)

Peerce, B.E., Wright, E.M. 1984. Sodium induced conformational changes in the glucose transporter of intestinal brush border membranes. *J. Biol. Chem.* **259:**14105–14112.

Peerce, B.E., Wright, E.M. 1987. Examination of the Na^+-induced conformational change of the intestinal brush border sodium-glucose symporter using fluorescent probes. *Biochemistry* **26:**4272–4279

Restrepo, D., Kimmich, G.A. 1985*a*. Kinetic analysis of mechanism of intestinal Na^+-dependent sugar transport. *Am. J. Physiol.* **248:**C498–C509

Restrepo, D., Kimmich, G.A. 1985*b*. The mechanistic nature of the membrane potential dependence of sodium-agar cotransport in small intestine. *J. Membrane Biol.* **87:**159–172

Roomans, G.M., Borst-Pauwels, G.W.F.H. 1978. Co-transport of anions and neutral solutes with cations across charged

biological membranes. Effects of surface potential on uptake kinetics. *J. Theor. Biol.* **73:**453–468

Roy, G., Wierzbicki, W., Sauvé, R. 1991. Membrane transport models with fast and slow reactions: General analytical solution for a single relaxation. *J. Membrane Biol.* **123:**105–113

Sanders, D. 1986. Generalized kinetic analysis of ion-driven cotransport systems: II. Random ligand binding as a simple explanation for non-Michaelian kinetics. *J. Membrane Biol.* **90:**67–87

Sanders, D., Hansen, U.P., Gradmann, D., Slayman, C.L. 1984. Generalized kinetic analysis of ion-driven cotransport systems: A unified interpretation of selective ionic effects on Michaelis parameters. *J. Membrane Biol.* **77:**123–152

Schultz, S.G. 1986. Ion-coupled transport of organic solutes across biological membranes. *In*: Physiology of Membrane Disorders. T.E. Andreoli, J.F. Hoffman, D.D. Fanestil, and S.G. Schultz, editors. pp. 283–294. Plenum, New York

Segel, I.H. 1975. Enzyme Kinetics. John Wiley, New York

Stevens, B.R., Fernandez, A., Hirayama, B., Wright, E.M., Kempner, E.S. 1990. Intestinal brush border membrane Na^+/glucose cotransporter functions *in situ* as a homotetramer. *Proc. Natl. Acad. Sci. USA* **87:**1456–1460

Stevens, B.R., Kaunitz, J.D., Wright, E.M. 1984. Intestinal transport of amino acids and sugars: Advances using membrane vesicles. *Annu. Rev. Physiol.* **46:**417–433

Supplisson, S. 1988. Etude du caractère électrogène et de la sensibilité au voltage du transport de D-glucose couplé au sodium à travers la membrane de vésicules de bordures en brosse intestinales de Cobaye et de Porc. Ph.D. Thesis, Université de Paris-Sud, Centre D'Orsay

Toggenburger, G., Kessler, M., Semenza, G. 1982. Phlorizin as a probe of the small-intestinal Na^+, D-glucose cotransporter. A model. *Biochim. Biophys. Acta* **688:**557–571

Turner, R.J., Silverman, M. 1981. Interaction of phlorizin and sodium with the renal brush border membrane D-glucose transporter: Stoichiometry and order of binding. *J. Membrane Biol.* **58:**43–55

Umbach, J., Coady, M.J., Wright, E.M. 1990. Intestinal Na^+/glucose cotransporter expressed in *Xenopus* oocytes is electrogenic. *Biophys. J.* **57:**1218–1224

Wierzbicki, W., Berteloot, A., Roy, G. 1990. Pre-steady-state kinetics and carrier-mediated transport: A theoretical analysis. *J. Membrane Biol.* **117:**11–27

Received 12 April 1991; revised 25 June 1991

Appendix

The model for the Na^+/glucose cotransporter involves 6 states (C_1, ..., C_6) which contains two closed loops of 4 states each (Fig. A1).

Derivation of the Steady-State Current Equation for a 6-State Ordered Binding Cotransport Model without Assuming Rapid Equilibrium

Current equations were derived using the graphical method of King and Altman (1956). Figure A1 shows the 15 different King-Altman patterns.

Thus the steady-state concentration of each carrier form is solved according to:

$$\frac{[C_x]}{C_T} = \frac{\sum_{j=1}^{15} \mathrm{KAT}_x^j}{\sum_{i=1}^{6}\sum_{j=1}^{15} \mathrm{KAT}_i^j} \qquad \text{(A1)}$$

where C_x (x = 1, ..., 6) is a given state of the carrier and $C_T = \frac{\text{number of carriers per oocyte}}{6.022 \times 10^{23}} \cdot \mathrm{KAT}_i^j$ is an individual King-Altman term with i being any carrier state and j one of the King-Altman patterns. Each term is the product of five pseudo first order rate constants (*see* Eqs. (A14) to (A19)).

Individual Rate Constants

Rapid equilibrium binding of Na^+ ions and rapid equilibrium binding of sugar was not assumed. Every reaction step between two carrier states was treated as a function of first order (k_{16}, k_{61}, k_{21}, k_{32}, k_{34}, k_{43}, k_{45}, k_{25}, k_{52}, k_{65}) or pseudo first order rate constants (k_{12}, k_{23}, k_{65}, k_{54}). The effect of voltage and ligand concentration (Na^+ ions or sugar) was accounted for in the calculation of the rate constants.

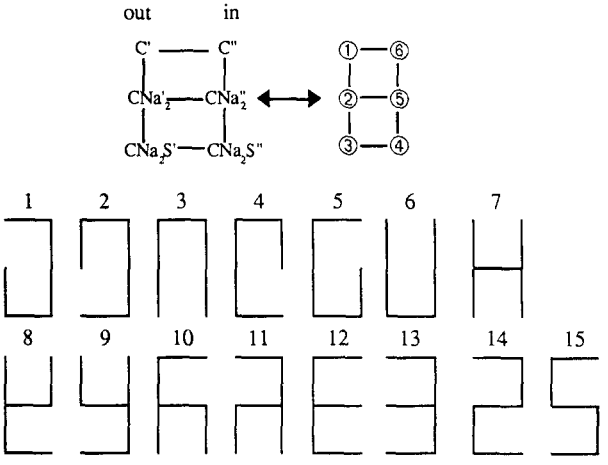

Fig. A1. Model, carrier states and the corresponding King-Altman patterns.

Voltage may influence both Na^+ ion binding and carrier translocation. The effect of membrane potential on rate constants was treated according to the Eyring theory of transition states, assuming a single and symmetrical energy barrier for each reaction step. We used the terminology introduced by Läuger and Jauch (1986) where α' and α'' describe the fraction of the membrane field between Na^+ ions and the Na^+ binding sites and δ characterizes the effect of membrane potential on carrier translocation, and by definition $\alpha' + \delta + \alpha'' = 1$.

Pseudo first order rate constants (sec^{-1}) are described by:

$$k_{16} = k_{16}^0 e^{(-z_c\delta\frac{\mu}{2})} = k_{16}^0 e^{(\delta\mu)} \tag{A2}$$

$$k_{61} = k_{61}^0 e^{(z_c\delta\frac{\mu}{2})} = k_{61}^0 e^{(-\delta\mu)} \tag{A3}$$

$$k_{12} = k_{12}^0[\mathrm{Na}]_o'' e^{(-nz_{\mathrm{Na}}\alpha''\frac{\mu}{2})} = k_{12}^0[\mathrm{Na}]_o^2 e^{(-\alpha''\mu)} = k_{12}^*[\mathrm{Na}]_o^2 \tag{A4}$$

$$k_{21} = k_{21}^0 e^{(nz_{\mathrm{Na}}\alpha'\frac{\mu}{2})} = k_{21}^0 e^{(\alpha'\mu)} \tag{A5}$$

$$k_{65} = k_{65}^0[\mathrm{Na}]_i'' e^{(nz_{\mathrm{Na}}\alpha''\frac{\mu}{2})} = k_{65}^0[\mathrm{Na}]_i^2 e^{(\alpha''\mu)} = k_{65}^*[\mathrm{Na}]_i^2 \tag{A6}$$

$$k_{56} = k_{56}^0 e^{(-nz_{\mathrm{Na}}\alpha''\frac{\mu}{2})} = k_{56}^0 e^{(-\alpha''\mu)} \tag{A7}$$

$$k_{23} = k_{23}^0[S]_o \tag{A8}$$

$$k_{54} = k_{54}^0[S]_i \tag{A9}$$

where k_{12}^* and k_{65}^* include the effect of voltage and

$$\mu = \frac{FV}{RT} \tag{A10}$$

where z_c is the valence of the ion binding site on the empty carrier ($z_c = -2$), n the apparent coupling coefficient ($n = 2$), z_{Na} the valence of sodium ions ($z_{\mathrm{Na}} = 1$), V, R, T and F have their usual meanings.

Microscopic Reversibility

The thermodynamic requirement for a microscopic reversibility (no accumulation of carrier can occur in the absence of driving force) imposes a constraint for the determination of one rate constant on each cycle. In our simulation program, k_{52} and k_{54}^0, were systematically calculated from the values of the other rate constants such as:

$$k_{52} = \frac{k_{12}^0 k_{25} k_{56}^0 k_{61}^0}{k_{21}^0 k_{16}^0 k_{65}^0} \tag{A11}$$

$$k_{54}^0 = \frac{k_{23}^0 k_{34} k_{45} k_{52}}{k_{43} k_{32} k_{25}}. \tag{A12}$$

Steady-State Carrier Concentrations

The conservation equation for all carrier species is given by:

$$C_T = [C]' + [CNa_2]' + [CNa_2S]' + [CNa_2S]'' + [CNa_2]'' + [C]''. \tag{A13}$$

The steady-state concentration of each carrier state could be estimated using the King-Altman procedure shown in Fig. A1. For simplicity, the KAT terms are given in the form: $\sum_{j=1}^{15} \mathrm{KAT}_x^j = \Sigma C_x$

$$\begin{aligned}\Sigma C_1 &= k_{21}k_{32}k_{43}k_{52}k_{61} + k_{21}k_{32}k_{45}k_{52}k_{61} + k_{21}k_{34}k_{45}k_{52}k_{61}\\ &+ k_{21}k_{32}k_{43}k_{54}k_{61} + k_{21}k_{32}k_{43}k_{56}k_{61} + k_{25}k_{32}k_{43}k_{56}k_{61}\\ &+ k_{21}k_{32}k_{45}k_{56}k_{61} + k_{25}k_{32}k_{45}k_{56}k_{61} + k_{21}k_{34}k_{45}k_{56}k_{61}\\ &+ k_{23}k_{34}k_{45}k_{56}k_{61} + k_{25}k_{34}k_{45}k_{56}k_{61} + k_{21}k_{32}k_{43}k_{52}k_{65}\\ &+ k_{21}k_{32}k_{45}k_{52}k_{65} + k_{21}k_{34}k_{45}k_{52}k_{65} + k_{21}k_{32}k_{43}k_{54}k_{65}\end{aligned} \tag{A14}$$

$$\begin{aligned}\Sigma C_2 &= k_{12}k_{32}k_{43}k_{52}k_{61} + k_{12}k_{32}k_{45}k_{52}k_{61} + k_{12}k_{34}k_{45}k_{52}k_{61}\\ &+ k_{12}k_{32}k_{43}k_{54}k_{61} + k_{12}k_{32}k_{43}k_{56}k_{61} + k_{12}k_{32}k_{45}k_{56}k_{61}\\ &+ k_{12}k_{34}k_{45}k_{56}k_{61} + k_{12}k_{32}k_{43}k_{52}k_{65} + k_{16}k_{32}k_{43}k_{52}k_{65}\\ &+ k_{12}k_{32}k_{45}k_{52}k_{65} + k_{16}k_{32}k_{45}k_{52}k_{65} + k_{12}k_{34}k_{45}k_{52}k_{65}\\ &+ k_{16}k_{34}k_{45}k_{52}k_{65} + k_{12}k_{32}k_{43}k_{54}k_{65} + k_{16}k_{32}k_{43}k_{54}k_{65}\end{aligned} \tag{A15}$$

$$\begin{aligned}\Sigma C_3 &= k_{12}k_{23}k_{43}k_{52}k_{61} + k_{12}k_{23}k_{45}k_{52}k_{61} + k_{12}k_{23}k_{43}k_{54}k_{61}\\ &+ k_{12}k_{25}k_{43}k_{54}k_{61} + k_{12}k_{23}k_{43}k_{56}k_{61} + k_{12}k_{23}k_{45}k_{56}k_{61}\\ &+ k_{12}k_{23}k_{43}k_{52}k_{65} + k_{16}k_{23}k_{43}k_{52}k_{65} + k_{12}k_{23}k_{45}k_{52}k_{65}\\ &+ k_{16}k_{23}k_{45}k_{52}k_{65} + k_{16}k_{21}k_{43}k_{54}k_{65} + k_{12}k_{23}k_{43}k_{54}k_{65}\\ &+ k_{16}k_{23}k_{43}k_{54}k_{65} + k_{12}k_{25}k_{43}k_{54}k_{65} + k_{16}k_{25}k_{43}k_{54}k_{65}\end{aligned} \tag{A16}$$

$$\begin{aligned}\Sigma C_4 &= k_{12}k_{23}k_{34}k_{52}k_{61} + k_{12}k_{25}k_{32}k_{54}k_{61} + k_{12}k_{23}k_{34}k_{54}k_{61}\\ &+ k_{12}k_{25}k_{34}k_{54}k_{61} + k_{12}k_{23}k_{34}k_{56}k_{61} + k_{12}k_{23}k_{34}k_{52}k_{65}\\ &+ k_{16}k_{23}k_{34}k_{52}k_{65} + k_{16}k_{21}k_{32}k_{54}k_{65} + k_{12}k_{25}k_{32}k_{54}k_{65}\\ &+ k_{16}k_{25}k_{32}k_{54}k_{65} + k_{16}k_{21}k_{34}k_{54}k_{65} + k_{12}k_{23}k_{34}k_{54}k_{65}\\ &+ k_{16}k_{23}k_{34}k_{54}k_{65} + k_{12}k_{25}k_{34}k_{54}k_{65} + k_{16}k_{25}k_{34}k_{54}k_{65}\end{aligned} \tag{A17}$$

$$\begin{aligned}\Sigma C_5 &= k_{12}k_{25}k_{32}k_{43}k_{61} + k_{12}k_{25}k_{32}k_{45}k_{61} + k_{12}k_{23}k_{34}k_{45}k_{61}\\ &+ k_{12}k_{25}k_{34}k_{45}k_{61} + k_{16}k_{21}k_{32}k_{43}k_{65} + k_{12}k_{25}k_{32}k_{43}k_{65}\\ &+ k_{16}k_{25}k_{32}k_{43}k_{65} + k_{16}k_{21}k_{32}k_{45}k_{65} + k_{12}k_{25}k_{32}k_{45}k_{65}\\ &+ k_{16}k_{25}k_{32}k_{45}k_{65} + k_{16}k_{21}k_{34}k_{45}k_{65} + k_{12}k_{23}k_{34}k_{45}k_{65}\\ &+ k_{16}k_{23}k_{34}k_{45}k_{65} + k_{12}k_{25}k_{34}k_{45}k_{65} + k_{16}k_{25}k_{34}k_{45}k_{65}\end{aligned} \tag{A18}$$

$$\begin{aligned}\Sigma C_6 &= k_{16}k_{21}k_{32}k_{43}k_{52} + k_{16}k_{21}k_{32}k_{45}k_{52} + k_{16}k_{21}k_{34}k_{45}k_{52}\\ &+ k_{16}k_{21}k_{32}k_{43}k_{54} + k_{16}k_{21}k_{32}k_{43}k_{56} + k_{12}k_{25}k_{32}k_{43}k_{56}\\ &+ k_{16}k_{25}k_{32}k_{43}k_{56} + k_{16}k_{21}k_{32}k_{45}k_{56} + k_{12}k_{25}k_{32}k_{45}k_{56}\\ &+ k_{16}k_{25}k_{32}k_{45}k_{56} + k_{16}k_{21}k_{34}k_{45}k_{56} + k_{12}k_{23}k_{34}k_{45}k_{56}\\ &+ k_{16}k_{23}k_{34}k_{45}k_{56} + k_{12}k_{25}k_{34}k_{45}k_{56} + k_{16}k_{25}k_{34}k_{45}k_{56}.\end{aligned} \tag{A19}$$

Steady-State Current Equation

The steady-state current equation is expressed as:

$$i = -z_c F(k_{16}[C]' - k_{61}[C]''). \tag{A20}$$

Equation (A20) was then solved for $[C]'$ and $[C]''$ using Eqs. (A1) and (A14) to (A19). The steady-state current equation can be rearranged both for zero-*trans* and nonzero-*trans* conditions as a function of the external sodium and sugar concentrations with $z_c = -2$ and $n = 2$:

$$i = 2F C_T \left[\frac{\varepsilon[\mathrm{Na}]_o^2[S]_o + \phi[\mathrm{Na}]_o^2 + \gamma}{\alpha + \beta[S]_o + \chi[\mathrm{Na}]_o^2 + [\mathrm{Na}]_o^2[S]_o}\right]. \tag{A21}$$

Under nonzero-*trans* conditions ($[\mathrm{Na}]_i > 0$ and $[S]_i > 0$), the macro constants are defined by:

$$\varepsilon = -\frac{1}{\lambda} k_{12}^* k_{23}^0 k_{34} k_{45} k_{56} k_{61} \tag{A22}$$

$$\phi = -\frac{1}{\lambda} k_{12}^* k_{56} k_{61}(k_{25}k_{34}k_{45} + k_{32}k_{25}k_{43} + k_{32}k_{25}k_{45}) \tag{A23}$$

$$\gamma = \frac{1}{\lambda} k_{16}k_{21}k_{65}(k_{34}k_{45}k_{52} + k_{32}k_{43}k_{52} + k_{32}k_{45}k_{52} + k_{32}k_{43}k_{54}) \tag{A24}$$

$$\begin{aligned}\alpha = \frac{1}{\lambda}\,&(k_{16}k_{21}k_{32}k_{43}k_{52} + k_{16}k_{21}k_{32}k_{45}k_{52} + k_{16}k_{21}k_{34}k_{45}k_{52}\\ &+ k_{16}k_{21}k_{32}k_{43}k_{54} + k_{16}k_{21}k_{32}k_{43}k_{56} + k_{16}k_{25}k_{32}k_{43}k_{56}\\ &+ k_{16}k_{21}k_{32}k_{45}k_{56} + k_{16}k_{25}k_{32}k_{45}k_{56} + k_{16}k_{21}k_{34}k_{45}k_{56}\\ &+ k_{16}k_{25}k_{34}k_{45}k_{56} + k_{21}k_{32}k_{43}k_{52}k_{61} + k_{21}k_{32}k_{45}k_{52}k_{61}\\ &+ k_{21}k_{34}k_{45}k_{52}k_{61} + k_{21}k_{32}k_{43}k_{54}k_{61} + k_{21}k_{32}k_{43}k_{56}k_{61}\\ &+ k_{25}k_{32}k_{43}k_{56}k_{61} + k_{21}k_{32}k_{45}k_{56}k_{61} + k_{25}k_{32}k_{45}k_{56}k_{61}\\ &+ k_{21}k_{34}k_{45}k_{56}k_{61} + k_{25}k_{34}k_{45}k_{56}k_{61} + k_{16}k_{21}k_{32}k_{43}k_{65}\\ &+ k_{16}k_{25}k_{32}k_{43}k_{65} + k_{16}k_{21}k_{32}k_{45}k_{65} + k_{16}k_{25}k_{32}k_{45}k_{65}\\ &+ k_{16}k_{21}k_{34}k_{45}k_{65} + k_{16}k_{25}k_{34}k_{45}k_{65} + k_{16}k_{32}k_{43}k_{52}k_{65}\end{aligned} \tag{A25}$$

$$+ k_{21}k_{32}k_{43}k_{52}k_{65} + k_{16}k_{32}k_{45}k_{52}k_{65} + k_{21}k_{32}k_{45}k_{52}k_{65} + k_{16}k_{34}k_{45}k_{52}k_{65} + k_{21}k_{34}k_{45}k_{52}k_{65} + k_{16}k_{21}k_{32}k_{54}k_{65} + k_{16}k_{25}k_{32}k_{54}k_{65} + k_{16}k_{21}k_{34}k_{54}k_{65} + k_{16}k_{25}k_{34}k_{54}k_{65} + k_{16}k_{21}k_{43}k_{54}k_{65} + k_{16}k_{25}k_{43}k_{54}k_{65} + k_{16}k_{32}k_{43}k_{54}k_{65} + k_{21}k_{32}k_{43}k_{54}k_{65}) \quad \text{(A25)}$$

$$\beta = \frac{1}{\lambda} k_{23}^0 (k_{16}k_{34}k_{45}k_{56} + k_{34}k_{45}k_{56}k_{61} + k_{16}k_{34}k_{45}k_{65} + k_{16}k_{34}k_{52}k_{65} + k_{16}k_{43}k_{52}k_{65} + k_{16}k_{45}k_{52}k_{65} + k_{16}k_{34}k_{54}k_{65} + k_{16}k_{43}k_{54}k_{65}) \quad \text{(A26)}$$

$$\chi = \frac{1}{\lambda} k_{12}^* (k_{25}k_{32}k_{43}k_{56} + k_{25}k_{32}k_{45}k_{56} + k_{25}k_{34}k_{45}k_{56} + k_{25}k_{32}k_{43}k_{61} + k_{25}k_{32}k_{45}k_{61} + k_{25}k_{34}k_{45}k_{61} + k_{32}k_{43}k_{52}k_{61} + k_{32}k_{45}k_{52}k_{61} + k_{34}k_{45}k_{52}k_{61} + k_{25}k_{32}k_{54}k_{61} + k_{25}k_{34}k_{54}k_{61} + k_{25}k_{43}k_{54}k_{61} + k_{32}k_{43}k_{54}k_{61} + k_{32}k_{43}k_{56}k_{61} + k_{32}k_{45}k_{56}k_{61} + k_{34}k_{45}k_{56}k_{61} + k_{25}k_{32}k_{43}k_{65} + k_{25}k_{32}k_{45}k_{65} + k_{25}k_{34}k_{45}k_{65} + k_{32}k_{43}k_{52}k_{65} + k_{32}k_{45}k_{52}k_{65} + k_{34}k_{45}k_{52}k_{65} + k_{25}k_{32}k_{54}k_{65} + k_{25}k_{34}k_{54}k_{65} + k_{25}k_{43}k_{54}k_{65} + k_{32}k_{43}k_{54}k_{65} \quad \text{(A27)}$$

$$\lambda = k_{12}^* k_{23}^0 (k_{34}k_{45}k_{56} + k_{34}k_{45}k_{61} + k_{34}k_{52}k_{61} + k_{43}k_{52}k_{61} + k_{45}k_{52}k_{61} + k_{34}k_{54}k_{61} + k_{43}k_{54}k_{61} + k_{34}k_{56}k_{61} + k_{43}k_{56}k_{61} + k_{45}k_{56}k_{61} + k_{34}k_{45}k_{65} + k_{34}k_{52}k_{65} + k_{43}k_{52}k_{65} + k_{45}k_{52}k_{65} + k_{34}k_{54}k_{65} + k_{43}k_{54}k_{65}). \quad \text{(A28)}$$

Assuming zero-*trans* conditions, ($[Na]_i = 0$, $[S]_i$, i.e. k_{65} and $k_{54} = 0$), the macro constants simplify further to:

$$\varepsilon = -\frac{1}{\lambda} k_{12}^* k_{23}^0 k_{34}k_{45}k_{56}k_{61} \quad \text{(A29)}$$

$$\phi = -\frac{1}{\lambda} k_{12}^* k_{25}k_{56}k_{61}(k_{32}k_{43} + k_{32}k_{45} + k_{34}k_{45}) \quad \text{(A30)}$$

$$\gamma = 0 \quad \text{(A31)}$$

$$\alpha = \frac{1}{\lambda} (k_{16} + k_{61})(k_{32}k_{43} + k_{32}k_{45} + k_{34}k_{45})(k_{21}k_{52} + k_{21}k_{56} + k_{25}k_{56}) \quad \text{(A32)}$$

$$\beta = \frac{1}{\lambda} k_{23}^0 k_{34}k_{45}k_{56}(k_{16} + k_{61}) \quad \text{(A33)}$$

$$\chi = \frac{1}{\lambda} k_{12}^* (k_{32}k_{43} + k_{32}k_{45} + k_{34}k_{45})(k_{25}k_{56} + k_{25}k_{61} + k_{52}k_{61} + k_{56}k_{61}) \quad \text{(A34)}$$

$$\lambda = k_{12}^* k_{23}^0 (k_{34}k_{45}k_{56} + k_{34}k_{45}k_{61} + k_{34}k_{52}k_{61} + k_{43}k_{52}k_{61} + k_{45}k_{52}k_{61} + k_{34}k_{56}k_{61} + k_{43}k_{56}k_{61} + k_{45}k_{56}k_{61}). \quad \text{(A35)}$$

Phenomenological Current Equations and Constants

Steady-state current Eq. (A21) can be rearranged as a sum of two phenomenological equations, as a function of either the external sugar, Eq. (A36), or the external sodium, Eq. (A40), concentration:

$$i = \left[\frac{I_{max}^S [S]_o}{K_{0.5}^S + [S]_o}\right] + \left[\frac{I_{max}^{S=0}}{K_{0.5}^S + [S]_o}\right] \quad \text{(A36)}$$

$$\begin{cases} I_{max}^S = 2FC_T \left[\dfrac{\varepsilon [Na]_o^2}{\beta + [Na]_o^2}\right] & \text{(A37)} \\ I_{max}^{S=0} = 2FC_T \left[\dfrac{\phi [Na]_o^2 + \gamma}{\beta + [Na]_o^2}\right] & \text{(A38)} \\ K_{0.5}^S = \left[\dfrac{\alpha + \chi [Na]_o^2}{\beta + [Na]_o^2}\right] & \text{(A39)} \end{cases}$$

where ε, ϕ, γ, α, β, and χ had been previously defined by Eqs. (A22) to (A35)

$$i = \left[\frac{I_{max}^{Na} [Na]_o^2}{[K_{0.5}^{Na}]^2 + [Na]_o^2}\right] + \left[\frac{I_{max}^{Na=0}}{[K_{0.5}^{Na}]^2 + [Na]_o^2}\right] \quad \text{(A40)}$$

$$\begin{cases} I_{max}^{Na} = 2FC_T \left[\dfrac{\phi + \varepsilon [S]_o}{\chi + [S]_o}\right] & \text{(A41)} \\ I_{max}^{Na=0} = 2FC_T \left[\dfrac{\gamma}{\chi + [S]_o}\right] & \text{(A42)} \\ K_{0.5}^{Na} = \left[\dfrac{\alpha + \beta [S]_o}{\chi + [S]_o}\right]. & \text{(A43)} \end{cases}$$

Phenomenological constants I_{max}^S and $K_{0.5}^S$ were generated from Eqs. (A38) and (A40), and phenomenological constants I_{max}^{Na} and $K_{0.5}^{Na}$ were generated from Eqs. (A41) and (A43). Under our experimental conditions $I_{max}^{Na=0}$ and $I_{max}^{S=0}$ were found to be negligible, which is confirmed when their value is calculated using the rate constants shown in Fig. 2.

Presteady-State Current: Numerical Integration Procedure

The time course of the carrier current in response to a step of voltage ΔV from a holding potential was estimated by numerical integration. The initial concentration of each carrier species was calculated according to Eqs. (A14) to (A19), assuming that the carrier distribution was at steady state at the holding potential ($t = 0$) just before the pulse of voltage. The time course of each carrier species was obtained by numerical integration of the following set of differential equations (A44) to (A49) with a time interval Δt between 10 and 50 μsec. The carrier current was calculated according to Eq. (A50).

$$\frac{d[C]'}{dt} = k_{61}[C]'' + k_{21}[CNa_2]' - (k_{16} + k_{12})[C]' \quad \text{(A44)}$$

$$\frac{d[CNa_2]'}{dt} = k_{12}[C]' + k_{52}[CNa_2]'' + k_{32}[CNa_2S]' - (k_{21} + k_{25} + k_{23})[CNa_2]' \quad \text{(A45)}$$

$$\frac{d[CNa_2S]'}{dt} = k_{23}[CNa_2]' + k_{43}[CNa_2S]'' - (k_{32} + k_{34})[CNa_2S]' \quad \text{(A46)}$$

$$\frac{d[CNa_2S]''}{dt} = k_{34}[CNa_2S]' + k_{54}[CNa_2]'' - (k_{43} + k_{45})[CNa_2S]'' \quad \text{(A47)}$$

$$\frac{d[CNa_2]''}{dt} = k_{25}[CNa_2]' + k_{45}[CNa_2S]'' + k_{65}[C]'' - (k_{52} + k_{54} + k_{56})[CNa_2]'' \quad \text{(A48)}$$

$$\frac{d[C]''}{dt} = k_{16}[C]' + k_{56}[CNa_2]'' - (k_{61} + k_{65})[C]''. \quad \text{(A49)}$$

The presteady-state current is given by the sum of all translocation steps involving the transfer of a net charge in the membrane:

$$i = -F[z_{Na}\alpha'(k_{12}[C]' - k_{21}[CNa_2]') + z_c\delta'(k_{16}[C]' - k_{61}[C]'') + z_{Na}\alpha''(k_{56}[CNa_2]'' - k_{65}[C]'')]. \quad \text{(A50)}$$